batteries

MDPI

Article

Performance Comparison of Intelligent Energy Management Strategies for Hybrid Electric Vehicles with Photovoltaic Fuel Cell and Battery Integration

Mohammed A. Albadrani [1,*], Ragab A. Sayed [2,*], Sabry Allam [2], Hossam Youssef Hegazy [3], Md. Morsalin [4], Mohamed H. Abdelati [5] and Samia Abdel Fattah [3]

[1] Department of Mechanical Engineering, College of Engineering, Qassim University, Buraydah 51452, Saudi Arabia
[2] Automotive and Tractors Technology Department, Faculty of Technology and Education, Capital University—Helwan Branch, Cairo 11511, Egypt; allam@techedu.helwan.edu.eg
[3] Electrical Technology Department, Faculty of Technology and Education, Capital University—Helwan Branch, Cairo 11511, Egypt; hossamyh@techedu.helwan.edu.eg (H.Y.H.); samiaabdalfatah@techedu.helwan.edu.eg (S.A.F.)
[4] Department of Electrical and Electronic Engineering, Hajee Mohammad Danesh Science and Technology University, Dinajpur 5200, Bangladesh; morsalin.2102217@std.hstu.ac.bd
[5] Automotive and Tractors Engineering Department, Faculty of Engineering, Minia University, Minya 61519, Egypt; m.hilal@mu.edu.eg
* Correspondence: moa.albadrani@qu.edu.sa (M.A.A.); ragab.mahmoud@techedu.helwan.edu.eg (R.A.S.); Tel.: +20-1002982796 (R.A.S.)

Abstract

This study presents an optimized and comparative investigation of four intelligent energy management strategies—Proportional–Integral–Derivative (*PID*), Fuzzy Logic Control (*FLC*), Equivalent Consumption Minimization Strategy (*ECMS*), and Artificial Neural Network (ANN)—applied to a photovoltaic–fuel cell–battery hybrid electric vehicle (*PV–FC–HEV*). A high-fidelity MATLAB/Simulink model integrates a 6 kW proton-exchange membrane fuel cell (*PEMFC*), a 500 W photovoltaic subsystem with MPPT, and a lithium-ion battery (LiB) pack. While 1000 W/m^2 represents Standard Test Conditions (STC), the level of 400 W/m^2 was specifically selected to simulate average cloudy conditions common in urban driving environments, rather than standard NOCT (800 W/m^2), to test the EMS's robustness under significantly reduced PV support and stressed battery conditions (initial SOC = 30%). While surface contamination and the resulting performance degradation significantly impact real-world results, this study assumes a clean surface to establish an idealized performance baseline for the control algorithms. However, the authors acknowledge that contaminant accumulation is a key factor; future work will incorporate a degradation factor (e.g., a 10–15% efficiency penalty) to evaluate the reliability of these EMS strategies under actual operating conditions. *ECMS* achieved the lowest hydrogen consumption, saving up to 10 L compared with *PID*, while ANN maintained the most stable state of charge (*SOC* > 80%), minimizing deep discharge cycles and improving operational stability. *FLC* provided balanced operation under fluctuating irradiance. Overall, ANN offered the most harmonized energy flow and dynamic stability, whereas *ECMS* maximized fuel economy. The findings provide practical guidance for designing sustainable and intelligent control systems in next-generation hybrid electric vehicles.

Keywords: intelligent energy management; hydrogen consumption optimization; *SOC* stability; multi-source collaboration; *HEV*; dynamic; performance

Check for updates

Academic Editor: Diego Iannuzzi

Received: 6 March 2026
Revised: 1 April 2026
Accepted: 9 April 2026
Published: 21 April 2026

Copyright: © 2026 by the authors. Licensee MDPI, Basel, Switzerland. This article is an open access article distributed under the terms and conditions of the Creative Commons Attribution (CC BY) license.

1. Introduction

The innovation of hybrid electric vehicles (HEVs) has emerged as one of the centerpieces in the automotive industry due to their potential in fuel saving and environmental protection [1,2]. The coupling of PV systems with fuel cells (FCs) and lithium-ion batteries demonstrates potential future developments to keep these vehicles sustainable. But efficient energy management still urgently needs to be solved, especially by coordinating these energy sources well so that the vehicle can give full play to their performance and make the life expectancy of the battery longer.

Energy management in HEVs is a complex task that requires the coordination of energy contributions from different sources to handle driving requirements, as well as to maximize the overall efficiency [3–5]. The development of solar power as a method for eliminating reliance on traditional fuel sources and decreasing the consumption of hydrogen in FC-based vehicles is being considered. There are, however, several challenges in combining PV with FCs and batteries, as far as adjusting to varying environmental conditions and the requirements of dynamic vehicle driving are concerned [6]. It should be pointed out that the efficient utilization of vehicle-mounted photovoltaic systems requires combined infrastructure-level collaborative optimization. Recent research shows that charging station-level photovoltaic-energy storage joint scheduling can significantly improve the penetration rate of renewable energy, indirectly enhancing the sustainability of vehicle-mounted energy systems. Parlak et al. [7] showed that PV–HEV integration can provide meaningful benefits, including reduced charging dependency, up to 12–32.5% carbon emission reduction, and extended usage time under favorable operating conditions, particularly in regions with low daily travel distances. It should be pointed out that the efficient utilization of vehicle-mounted photovoltaic systems requires combined infrastructure-level collaborative optimization. Recent research shows that charging station-level photovoltaic-energy storage joint scheduling can significantly improve the penetration rate of renewable energy, indirectly enhancing the sustainability of vehicle-mounted energy systems [8]. Therefore, PV integration is best regarded as a complementary energy contributor whose effectiveness strongly depends on intelligent energy management and usage patterns.

Recently, the proposed load-side self-coordination control in distribution network scenarios has further confirmed the universal value of multi-source coordination in improving system robustness [8]. Recent research has made considerable progress on the energy management strategies (EMS) of hybrid systems [9]. Notably, control techniques [such as *PID, FLC, ECMS*, etc.] have been commonly used to improve the power-allocation efficiency between various energy sources of HEVs [3]. Such methodology is designed to improve overall vehicle performance by increasing fuel efficiency, extending battery life, reducing H_2 consumption from FC, and maintaining ESS over time. The various control strategies employed in HEVs are illustrated in Figure 1.

While surface contamination and the resulting performance degradation significantly impact real-world results, this study assumes a clean surface to establish an idealized performance baseline for the control algorithms. However, the authors acknowledge that contaminant accumulation is a key factor; future work will incorporate a degradation factor (e.g., a 10–15% efficiency penalty) to evaluate the reliability of these EMS strategies under actual operating conditions.

As shown in Figure 1, the strategies are broadly classified into three main categories: rule-based, optimization-based, and learning-based approaches. Rule-based strategies rely on predefined control rules and heuristic logic, typically offering simple implementation and real-time feasibility [10]; in this study, *PID* and *FLC* fall under this category. Optimization-based strategies determine optimal power distribution by minimizing a predefined cost function [11]; *ECMS* belongs to this class because it minimizes instantaneous

fuel consumption. Learning-based strategies employ data-driven or artificial intelligence techniques to adaptively manage power flow [12]; accordingly, the ANN-based controller employed in this work falls within this category. This classification provides a structured framework for comparing the operational characteristics and performance of the selected energy management strategies.

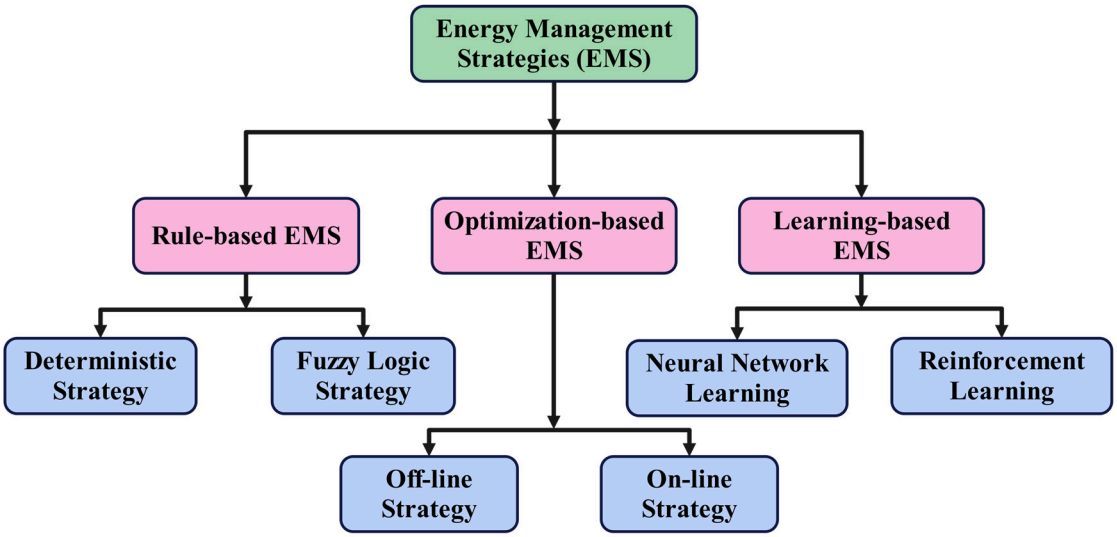


Figure 1. The strategies are broadly classified into three main categories: rule-based, optimization-based, and learning-based approaches.

Early *EMS* development was dominated by conventional rule-based controllers, among which *PID* controllers were extensively applied due to their simplicity, ease of implementation, and low computational requirements [13]. Fares et al. [14] proposed an LP-based *EMS* combined with a *PID* controller for an *HEV* powered by a hybrid *FC*–battery. In their approach, efficient power allocation among the energy sources was achieved using a two-stage control methodology, where LP was employed for optimal power distribution and an online *PID* controller was utilized to regulate system dynamics and ensure stable operation. However, *PID*-based *EMS* are highly dependent on fixed gains and lack adaptability under nonlinear system dynamics, load variations, and diverse driving cycles, which limits their effectiveness in complex hybrid energy systems [15]. To overcome these limitations, *FLC* emerged as an intelligent rule-based EMS [16,17]. Tao et al. [18] proposed a flexible complexity-reduced *PID*-like fuzzy controller. Their proposed approach achieved improved control performance and stability compared to classical *PID* and conventional complexity-reduced *PID*-like fuzzy controllers. FLC is an alternative solution that incorporates human expertise through linguistic rules and membership functions [19]. EMS is improved by handling uncertainties and nonlinearities of the vehicle system without requiring an accurate mathematical model [16]. Numerous studies have demonstrated that FLC-based EMS outperform deterministic strategies in terms of fuel economy, smoother power distribution, and battery state-of-charge (*SOC*) regulation [16,20]. H. D. Lee et al. [21] proposed a FLC for a parallel HEV with the objectives of improving vehicle e drivability and maintaining battery charge balance. Brahma et al. [22] developed an *HEV* modeling framework based on *FLC* aimed at optimizing fuel consumption. Baumann et al. [23] further demonstrated that *FLC* effectively improves fuel economy. Their proposed *FLC* maintains robust control performance under nonlinear conditions, ensuring its applicability to practical *HEV*.

Beyond heuristic approaches, optimization-based *EMS* have been widely adopted due to their strong theoretical foundation in optimal control. Paganelli et al. [24] proposed

ECMS first for a parallel *HEV*. *ECMS* translates electrical energy usage into an equivalent fuel consumption using an equivalence factor (*EF*), enabling real-time minimization of energy cost while achieving near-global optimality [24]. Compared to rule-based methods, *ECMS* has shown significant improvements in hydrogen consumption reduction from *FC* and battery lifespan extension [25]. Recent research has focused on adaptive and predictive variants of *ECMS* to address its sensitivity to driving conditions and EF selection, further enhancing its robustness [26,27]. In parallel, learning-based *EMS* using ANN have gained increasing attention as a powerful data-driven solution, which are capable of learning complex nonlinear relationships between vehicle states and optimal power-split decisions [28–30]. ANN-based *EMS* can be trained offline using optimal control results or real driving data and deployed online to provide adaptive and intelligent control under varying operating conditions [31].

The application of multilayer perceptrons (MLPs) in one-stage energy management systems has also received great attention [32,33]. Using machine learning, an ANN can react to current driving conditions, determine efficiently from a range of scenarios, and continuously change the balance between the internal combustion engine, battery, and fuel cell output [34,35]. This flexibility has been shown to enhance performance across a wide range of driving environments, resulting in more efficient energy consumption and lower peak current demand, thereby reducing operational stress on the battery [36].

Other methods for the *HEV* control combined with renewable energy sources like solar energy have been confirmed as well and work well to reduce reliance on fuel cells [37]. With the help of an intelligent energy management system, our photovoltaic subsystem can make a valuable contribution to meeting the vehicle's energy needs and reducing fuel consumption. By recharging the battery when solar irradiance is abundant, the PV system can facilitate not only vehicle propulsion but also contribute to greater energy independence, particularly in congested urban regions where solar availability varies from hour to hour.

Developments in battery *SOC* estimation have been paramount to the enhancement of the power management of hybrid systems [38]. Precise *SOC* estimation is important for power distribution optimization and battery overcharge/draining [39]. Recent physical field monitoring technologies (such as ultrasonic reflection wave methods) provide a non-destructive observation dimension of the battery's internal state, which can compensate for the measurement error limitations of traditional data-driven methods, further improving *SOC* control stability and lifespan prediction accuracy [40]. This is essential to ensuring the effectiveness of the hybrid system, as it reduces battery deterioration and increases vehicle efficiency [41]. Recent physical field monitoring technologies (such as ultrasonic reflection wave methods) provide a non-destructive observation dimension of the battery's internal state, which can compensate for the measurement error limitations of traditional data-driven methods, further improving SOC control stability and lifespan prediction accuracy [42]. In addition, the lithium-ion battery (LiB) aging and degradation represent critical challenges in HEV applications, as they directly affect system longevity, efficiency, and operational cost [43–45]. Lithium-ion batteries (LiBs) undergo performance decline over time due to both cycle aging and calendar aging [46]. These degradation mechanisms lead to capacity fading, increased internal resistance, and reduced power capability [47]. It also shortens the battery's usable lifespan and necessitates more frequent replacement or maintenance [48]. Modern battery management systems (BMS) increasingly incorporate aging-aware control strategies that monitor state of health (SOH) and adjust operating conditions [49]. These approaches often involve predictive models, health estimation techniques, and optimized charging protocols [50]. They highlight the importance of integrating

battery degradation considerations into advanced energy management frameworks for multi-source *HEV* powertrains [51].

Although fuel cell technology has advanced significantly over the past few decades, numerous obstacles remain to its commercialization, including the limited lifespan of fuel cells [52–54]. In particular, over extended periods of use, fuel cells will gradually lose performance. Performance degradation is induced by multiple variables, such as electrode material degradation, catalyst loss, mechanical damage to the membrane electrode assembly, and changes in operating conditions [55,56]. In addition to reducing fuel cell efficiency and output power, performance deterioration also shortens the cells' lifespan and raises maintenance and replacement expenses [57]. Therefore, improving fuel cell utilization through advanced control and energy management strategies in hybrid electric vehicles is essential to mitigate performance degradation, extend operational lifetime, and enhance overall system efficiency.

Even though some progress has been achieved, there is still much room to improve the management of multiple energy sources for *HEVs*, particularly in scenes with a varied environment. Even though the further development of each energy source has been combined separately in most studies [28,58–61], we find that integrated optimization is still a challenging issue due to the complex interrelation among PV, fuel cells, and batteries for practical driving patterns. Furthermore, the influence of solar radiation and driving profiles on energy management strategies is still an aspect that needs further investigation.

To overcome these challenges, more robust and flexible energy management systems adapted to complex multi-source hybrid systems will be addressed in future studies. This will involve better integration of renewable energy sources, more efficient power split algorithms, and the further refinement of battery management to continue maximizing operational life and performance.

2. System Description of PV–FC–Battery HEV

2.1. Overall Architecture

The photovoltaic (PV)–fuel cell (FC)–battery hybrid electric vehicle (PV–FC–Battery HEV) combines multiple energy sources and power electronic interfaces into a single, supervisory-controlled system capable of efficient and reliable propulsion. The plant consists of rooftop PV modules with Maximum Power Point Tracking (MPPT), a proton exchange membrane fuel cell (PEMFC) stack via a DC–DC boost converter, a LiB pack, a permanent magnet synchronous motor (PMSM) drive, and vehicle dynamics block, all regulated by an intelligent energy management system (EMS). All system components and models used in this study are implemented in MATLAB/Simulink environment and are not based on specific commercial manufacturers.

The PV field absorbs solar irradiation and transforms it into a voltage and current output and is interfaced with the DC bus through an MPPT converter, which regulates its operating point so as to maximize energy capture [62,63]. At low load or idle conditions, the surplus PV power was used to charge the battery, which effectively reduced hydrogen consumption and further improved energy self-sufficiency, especially under high irradiance conditions.

The PEMFC stack provides the primary energy source for propulsion and auxiliary power, which is supplied to meet the demand of DC via a boost converter controlled by a current or power control loop [64]. The fuel cell itself can drive the vehicle and assist in battery recharging at times when load demand is less than stack potential, with hydrogen flow governed using pressure-regulator and flow-control regulators to ensure safe and optimal performance [65].

The DC bus is coupled to a LiB pack, which works as an additional energy storage with high power density and quick dynamic response. It provides maximum power during acceleration, regenerative braking energy absorption, and smooths short-term load fluctuations, contributing to performance and protection of the components through transients from a fuel cell.

PMSM linked to the drivetrain provides traction and can be driven by a bi-directional voltage source inverter with vector control for torque and speed command. The vehicle dynamics block represents longitudinal motion (traction, aerodynamic drag, rolling resistance, and inertia-related effects) using typical characteristics such as mass of the vehicle, frontal area, and drivetrain type.

A supervisory EMS is the top control level that has access to instantaneous data of vehicle speed, requested power, PV-fed power, fuel cell status, and battery SOC. It compares the required load to system-generated data of PV, battery, and fuel cell powers calculated. Here, it calculates reference fuel cell power, seeking to coordinate contributions between the battery and PV in order to meet demand while minimizing consumption and maintaining SOC in an acceptable range.

Figure 2 provides a schematic representation of the PV–FC–Battery HEV structure, showing the interconnection of the PV array, PEMFC stack, battery pack, motor drive, and EMS on the common DC bus. All energy sources are integrated via a common DC bus maintained at a nominal voltage of 144 V to ensure stable power distribution.

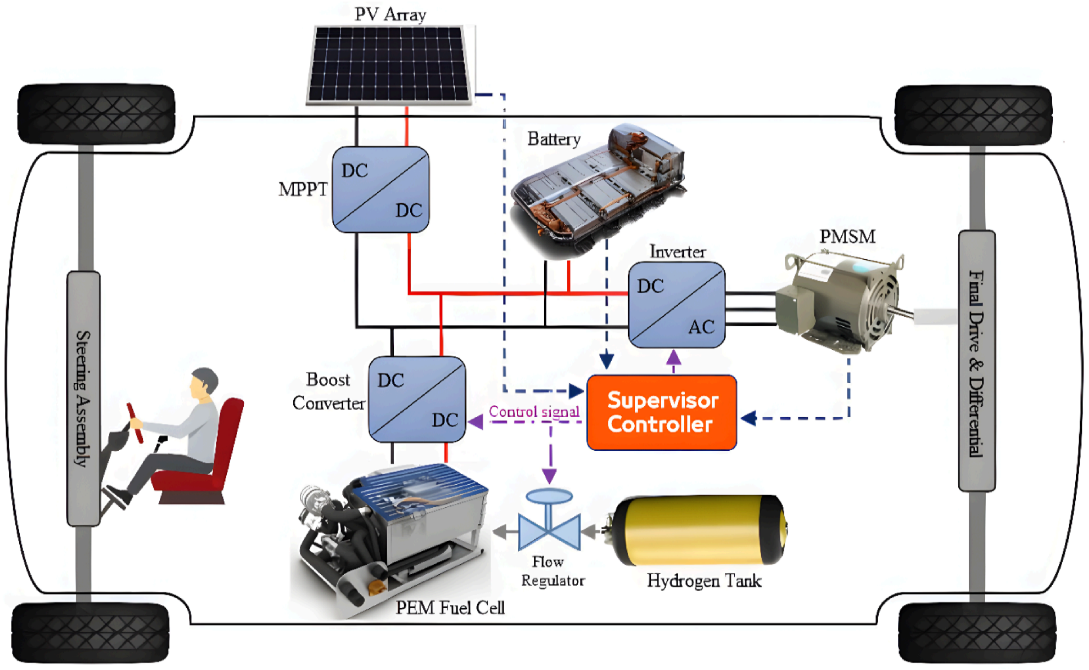


Figure 2. System architecture diagram of PV-FC-Battery HEV [66].

2.2. Photovoltaic Subsystem and MPPT

The photovoltaic (PV) subsystem is characterized by an equivalent single-diode circuit representation that describes the nonlinear current–voltage characteristics of the cells and depends on irradiance level and temperature [67]. The PV array current and voltage are described by the single-diode equation, which involves photocurrent, diode saturation current, series resistance, and temperature-dependent thermal voltage to achieve a precise model of the array under changing climatic conditions [68].

The I–V curve of a PV array has an optimum Maximum Power Point (MPP) at any irradiance–temperature condition in which the product of voltage and current is maximum.

The short-circuit current is found to increase rather critically, with increasing solar irradiance, compared to a moderate increase observed in e-motive voltage, and temperature variations also found to have profound influences on the open circuit voltage, which leads to decreasing maximum power at higher cell temperatures.

The MPPT DC–DC converter connected with the PV array allows the extraction of the maximum available power continuously. The MPPT controller changes the operating voltage to perturb and record the output power as a function of this perturbation, adjusting the duty cycle until it finds the MPP by tracking, for example, using a Perturb and Observe (P&O) algorithm.

With this structure, the PV subsystem can assist both propulsion and battery charging optimally under various irradiance profiles (sunny, cloudy, or no sun at night). Figure 3 illustrates the integrated configuration of the PV array, fuel cell, and battery system coordinated by the energy management system (EMS).

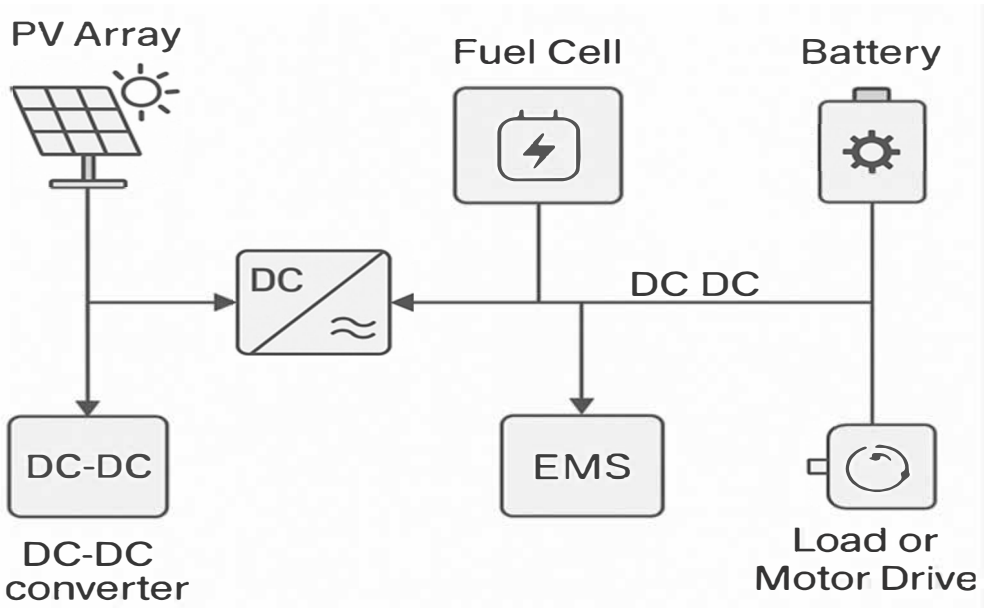


Figure 3. Integrated PV array, FC, and battery with EMS of HEV.

2.3. Fuel Cell Subsystem

The PEM FC subsystem is assumed to be characterized by dynamic voltage–current curves representing contributions from activation, ohmic, and concentration losses. The stack output voltage is represented as a subtraction between the open-circuit voltage and different overpotentials, which are logarithmic in current density, accounting for the electrochemical kinetics and the internal resistive losses.

A typical stack voltage relation can be written in the following form:

$$V_{\mathrm{FC}} = E_{\mathrm{OC}} - N_A \ln\left(\frac{i_{\mathrm{FC}}}{i_0}\right) \frac{1}{\frac{sT_{\mathrm{d}}}{3} + 1} - Ri_{\mathrm{FC}} \quad (1)$$

where E_{OC} is open-circuit voltage, A is the Tafel slope, i_0 is the exchange current, and R is the internal resistance. Fuel utilization rates and stack thermodynamics were parameterized based on [36–40]. To ensure the fidelity of the fuel cell model, parameters were identified using an accurate estimation method for PEMFC voltage models, ensuring the simulation aligns with experimental polarization curves.

The fuel cell is connected to the DC bus via a unidirectional DC–DC boost converter that regulates the output voltage and power delivered to the traction system. A

proportional–integral (PI) controller typically governs the converter, adjusting the duty cycle to track a reference fuel cell current or power command issued by the EMS.

Nominal design parameters for the PEMFC stack include a rated power of approximately 6 kW with a specific number of series-connected cells and an efficiency level suitable for automotive applications. These parameters are selected to match the vehicle power demand and to operate in a region that balances efficiency, durability, and hydrogen utilization.

In the overall architecture, the fuel cell acts as the leading energy provider, supplementing the PV subsystem and working in coordination with the battery to satisfy both steady-state and transient power requirements. Table 1 presents the nominal design parameters of the proton exchange membrane fuel cell (PEMFC) stack, including rated power, number of cells, efficiency, and other key specifications used in the PV–FC–Battery hybrid electric vehicle model.

Table 1. The parameters for PEMFC.

Parameter	Value	Unit
Operating temperature	65	°C
Nominal voltage	45	Volt
Nominal power	4.2	kW
Fuel supply pressure	1.5	bar
Peak power	6	kW
Number of cells	65	Piece
Nominal stack efficiency	55	%

2.4. Battery Model

The lithium-ion battery (LiB) pack is represented by an equivalent circuit model (ECM) that captures its dynamic voltage response as a function of SOC, current, and internal resistance, as shown in Figure 4.

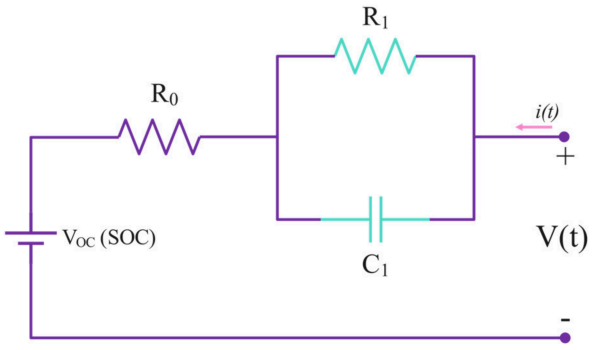


Figure 4. Dynamic model of the battery [69].

The instantaneous battery $SOC(t)$ of the *ECM* in Figure 4 is given as

$$SOC(t) = SOC(t_0) + \int_{t_0}^{t} \frac{1}{3600Q} i(t)dt \quad (2)$$

where Q is the nominal capacity of the cell (in Ah). The voltage Vc_1 across the R_1C_1 circuit is given by

$$\frac{dVc_1(t)}{dt} = -\frac{1}{R_1C_1} Vc_1(t) + \frac{1}{C_1} i(t) \quad (3)$$

Finally, after knowing the $SOC(t)$, Vc_1 and internal resistance R_0, the terminal voltage V can be calculated as

$$V(t) = V_{OC}(SOC(t)) + R_0 i(t) + Vc_1(t) \quad (4)$$

The model parameters are chosen to reproduce key behaviors such as voltage drop under load, recovery during rest, and *SOC* evolution during charge and discharge cycles. The MATLAB (R2018a) model of the battery used in this research is given by ref. [70].

The pack is configured to provide a nominal DC bus voltage on the order of 144 V with a specified capacity (e.g., 9.6 Ah), realized through an arrangement of series and parallel cell modules. This strategy guarantees maximum available energy storage for the purposes of propulsion, regenerative braking utilization, and transient power variations to be managed without reaching unsafe operating condition limits.

Battery *SOC* is updated by integrating the current over time, with charge and discharge efficiency factors reflecting conversion losses. Upper and lower *SOC* bounds are imposed to prevent overcharge and deep discharge, protecting battery health and prolonging cycle life, while the *EMS* enforces these limits by modulating fuel cell and PV contributions.

Within the PV–FC–Battery HEV, the battery primarily handles fast dynamics and short-duration events, such as acceleration, deceleration, and gridless operation under variable irradiance, complementing the slower fuel cell subsystem. Its interaction with the PV and fuel cell subsystems is managed on the common DC bus. Figure 5 illustrates the proposed electrical architecture of the PV–FC–Battery hybrid electric vehicle, showing the interconnection of the photovoltaic array, FC stack, battery pack, DC–DC converters, and supervisory energy management system on the common DC bus.

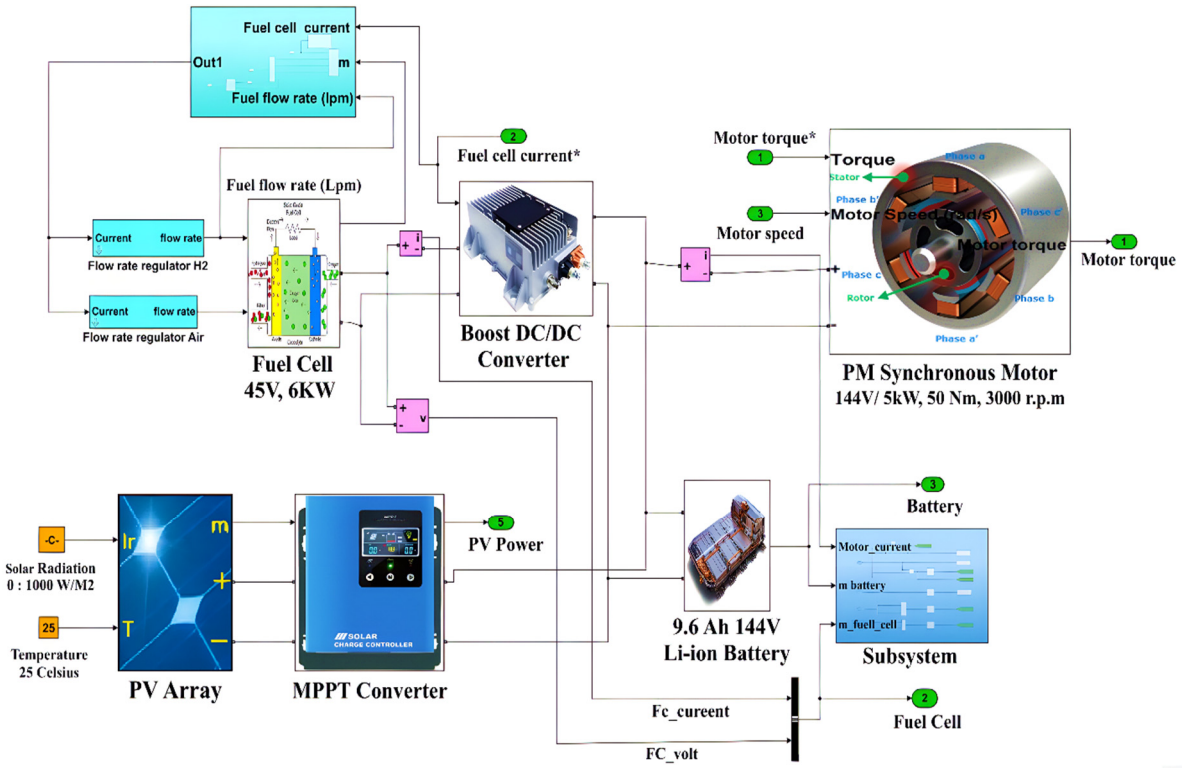


Figure 5. The proposed strategy was validated via Controller Hardware-in-the-Loop (CHiL) testing to ensure real-time execution stability. * Indicates the measured signals used for system monitoring [71].

2.5. Motor and Vehicle Dynamics

Traction power is delivered by a permanent magnet synchronous motor (PMSM) coupled to the vehicle drivetrain. The PMSM is driven by a three-phase inverter implementing vector (field-oriented) control to regulate torque and speed according to driver demand and vehicle operating conditions.

The motor is characterized by its rated power and torque, with typical values in the order of several kilowatts and tens of newton-meters, selected to match the vehicle performance requirements. The control system achieves maximum responsiveness in a wide speed range, providing smooth acceleration and deceleration while transferring the regenerative braking force.

Standard vehicle longitudinal dynamics are modeled considering the effects of wheel traction force, aerodynamic drag, rolling resistance, and inclination components due to gravitational forces on both ascending and descending slopes. Vehicle mass, frontal area, aerodynamic drag coefficient, wheel radius, and final drive ratio are important parameters that describe the relationship between motor torques and vehicle accelerations.

These parameters are combined in a design table, which defines the ratings and physical properties of the components, for uniform simulation of the WLTP driving cycle and other operation conditions. Table 2 summarizes the consolidated design parameters of the PV–FC–Battery hybrid electric vehicle, including vehicle mass, frontal area, aerodynamic drag coefficient, wheel radius, final drive ratio, and specifications for the PEMFC stack, PV array, battery pack, and PMSM. All energy sources (PV, FC, and battery) are integrated via a common DC bus maintained at a nominal voltage of 144 V to ensure stable power distribution. The table explicitly lists Vehicle Weight (800 kg), Motor Peak Power, and the specific drive cycle name (WLTP Class 1). The vehicle speed from the WLTP Class 1 cycle is converted into power demand ($P_{\text{subscriped:demand}}$) using longitudinal dynamics, accounting for a vehicle mass of 800 kg and an aerodynamic drag coefficient of 0.36.

Table 2. Consolidated design parameters for PV–FC–HEV model.

Component	Specification	Value/Unit	DC Bus Nominal Voltage	Drive Cycle	References
PEMFC nominal power	6 kW	65 cells, 55% efficiency	144 V	WLTP Class 1	[72]
PV array output	500 W	MPPT @ 1000 W/m^2	144 V	WLTP Class 1	[62,63,73]
Battery voltage/capacity	144 V/9.6 Ah	10 modules × 4 cells	144 V	WLTP Class 1	[74]
Motor type/torque	PMSM/50 Nm 3000 rpm	—	144 V	WLTP Class 1	[75]
Vehicle mass/frontal area	800 kg/2.3 m^2	—	144 V	WLTP Class 1	[76]
Aerodynamic drag coefficient	0.36	—	144 V	WLTP Class 1	[76]
Final drive ratio	3.0	—	144 V	WLTP Class 1	[76]

3. Mathematical Optimization Model

Building on the PV–FC–Battery HEV architecture described in Section 2, this section develops a mathematical optimization model that formulates the power-split problem over a discretized driving horizon.

3.1. Problem Definition

The objective of the mathematical model is to minimize the total fuel-cell energy (hydrogen consumption) over a finite time horizon by determining the optimal power contribution from the fuel cell, battery, and photovoltaic (PV) unit.

3.2. Time Discretization

The time horizon is divided into N steps of duration Δt: $k = 0, 1, 2, \ldots, N$.

3.3. Decision Variables

At each time step k,

- Fuel cell power: $P_{\mathrm{FC}}(k)$;
- Battery power (positive = discharge, negative = charge): $P_{\mathrm{bat}}(k)$;
- PV utilized power: $P_{\mathrm{PV}}(k)$;
- Battery state of charge: $SOC(k)$.

3.4. System Constraints

Battery constraints:

$$SOC_{\min} \leq SOC(k) \leq SOC_{\max} \tag{5}$$

$$P_{\mathrm{bat,ch}}^{\min} \leq P_{\mathrm{bat}}(k) \leq P_{\mathrm{bat,dis}}^{\max} \tag{6}$$

Fuel-cell constraints:

$$P_{\mathrm{FC}}^{\min} \leq P_{\mathrm{FC}}(k) \leq P_{\mathrm{FC}}^{\max} \tag{7}$$

$$|P_{\mathrm{FC}}(k) - P_{\mathrm{FC}}(k-1)| \leq R_{\mathrm{FC}}\Delta t \tag{8}$$

PV constraints:

$$0 \leq P_{\mathrm{PV}}(k) \leq P_{\mathrm{PV,avail}}(k) \tag{9}$$

3.5. SOC Dynamics

The discrete-time *SOC* dynamics are

$$SOC(k+1) = SOC(k) - \frac{P_{\mathrm{bat}}(k)\Delta t}{3600 E_{\mathrm{bat}}} \tag{10}$$

where E_{bat} is the nominal battery energy in Wh.

3.6. Power Balance

At each step, the power balance must hold

$$P_{\mathrm{FC}}(k) + P_{\mathrm{bat}}(k) + P_{\mathrm{PV}}(k) = P_{\mathrm{dem}}(k) \tag{11}$$

3.7. Boundary Conditions for Battery SOC

$$\left\{ \begin{matrix} SOC(0) = SOC_{init} \\ SOC(N) \geq SOC_{int} \end{matrix} \right\} \tag{12}$$

3.8. Final Formulation

Minimize total fuel-cell energy over the horizon:

$$\min \sum_{k=0}^{N-1} P_{\mathrm{FC}}(k)\Delta t \tag{13}$$

The complete optimization problem is formulated as

$$\min_{P_{FC},P_{bat},P_{PV},SOC}\{P_{FC}(k)+P_{bat}(k)+P_{PV}(k)=P_{dem}(k)\} \tag{14}$$

for all $k=0,1,\ldots,N-1$.

4. Intelligent Energy Management Strategies (PID, FLC, ECMS, ANN)

4.1. Role of EMS in PV–FC–HEV

The energy management system (*EMS*) coordinates real-time power sharing among the fuel cell (*FC*), battery, and photovoltaic (*PV*) array to meet vehicle load demands while minimizing hydrogen consumption and maintaining the battery state of charge (*SOC*) within optimal limits.

4.2. PID Controller

The *PID* controller regulates the fuel cell current based on the instantaneous error between the required and measured power. The control law is given by

$$u(t)=K_p\cdot e(t)+K_i\int_0^t e(\tau)d\tau+K_d\frac{d}{dt}e(t) \tag{15}$$

where $e(t)$ is the error, and K_p, K_i, K_d are the proportional, integral, and derivative gains, respectively.

The *PID* controller is fast and easy to tune but lacks adaptability under fluctuating irradiance and load conditions.

Figure 6 shows the block diagram of the PID controller structure used for regulating the fuel cell current/power in the *PV–FC*–Battery HEV system. Figure 7 illustrates the response of the *PID* controller under different operating conditions, highlighting its fast but less adaptive behavior.

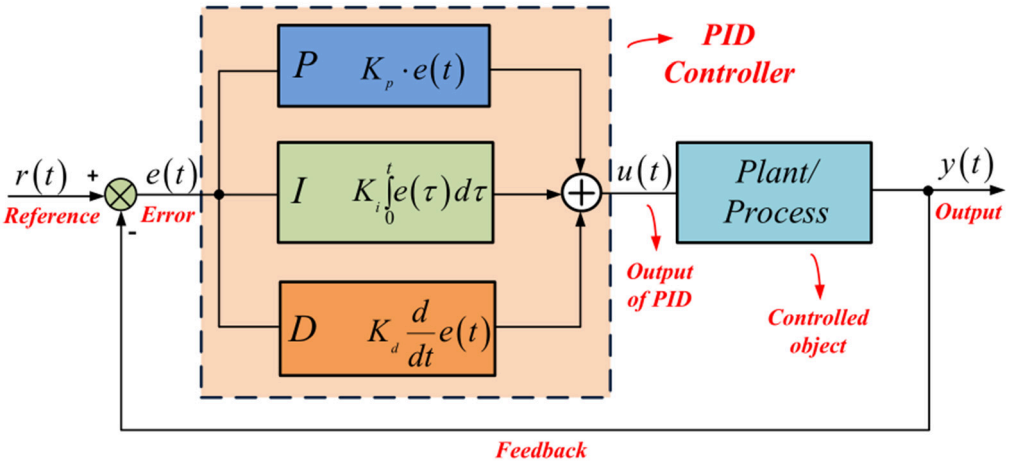


Figure 6. The *PID* controller employed in a closed-loop system.

4.3. Fuzzy Logic Controller (FLC)

The FLC uses rule-based linguistic decision-making for power allocation. The inputs are *PV* power (*PPV*), battery state of charge (*SOC*), and power demand (Pdemand). The output is the reference fuel cell power (PFC). Membership functions for *PPV*, *SOC*, and Pdemand are defined as LOW/MID/HIGH, VS/S/M/L/VL, and ZE/VS/.../VL, respectively.

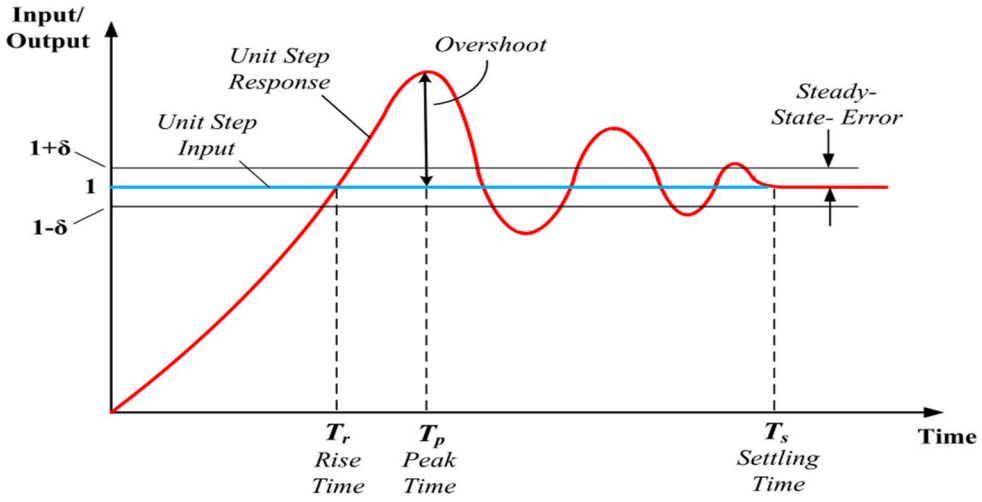


Figure 7. Unit step input/response of a closed-loop system.

Figure 8 displays the membership functions used in the *FLC* for *PV* power, *SOC*, and power demand, which are the inputs to the fuzzy inference system.

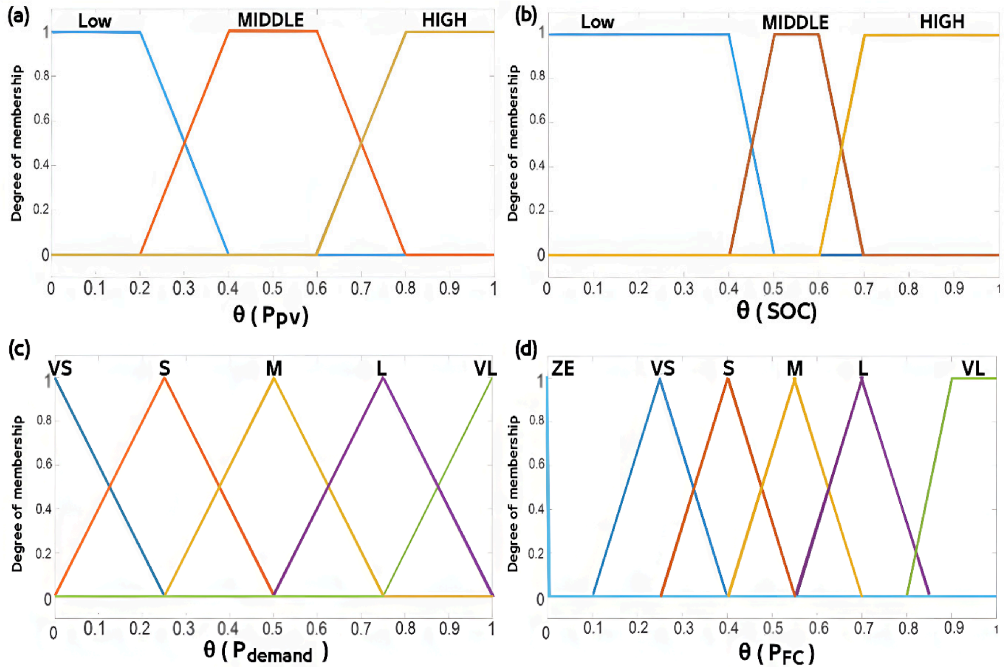


Figure 8. Fuzzy membership functions for (**a**) *PV* power (P_{PV}), (**b**) battery *SOC*, (**c**) power demand. (Pdemand), and (**d**) FC power output (P_{fc}).

4.4. Equivalent Consumption Minimization Strategy (ECMS)

The *ECMS* minimizes the total fuel-equivalent cost under the power balance among different energy sources (e.g., Battery, *PV*, *FC*) as in Equation (8).

It works in this study based on three real-time inputs:

1. Pdemand: The total power required by the vehicle's motor at any moment.
2. *SOC*: The battery's state of charge (from 0 to 100%).
3. PPV: Available solar energy (from solar panels, in kilowatts).

Why is this strategy needed?

- Battery protection: If the battery is used too much when it is already low on charge, it may degrade faster.

- Fuel efficiency: We want to avoid using nitrogen unnecessarily when the battery is healthy or there is enough solar power.
- Energy optimization: A smart control system helps balance the load between both sources efficiently, improving range, performance, and sustainability.

The following cost-based optimization is inside a MATLAB Function Block:

$$\text{cost} = \text{m}_{\text{H}_2} + m_{bat} \tag{16}$$

where m_{H_2} is equivalent mass of hydrogen consumed, and m_{bat} is the equivalent battery energy, adjusted with *SOC* penalty.

We minimize this cost by testing a range of P_{H2} values and selecting the one with the lowest cost.

The battery conversion factor is as follows:

$$s = \frac{3.6}{\eta_{batt} . Q_{lhv}} \tag{17}$$

where η_{batt} is the battery efficiency, and Q_{lhv} is the lower heating value of hydrogen.

The penalty factor based on *SOC* is

$$penalty = 1 - \left(\frac{SOC - SOC_{target}}{\frac{SOC_{max} - SOC_{min}}{2}} \right)^a \tag{18}$$

where a is the control's steepness.

The fuel cell hydrogen power consumption equation is

$$P_{fc} = \frac{P_{H2}}{\eta_{H2} . Q_{lhv}} \tag{19}$$

where Q_{lhv} is the lower heating value of H_2, and η_{H2} is the efficiency of the hydrogen engine.

The final cost function is

$$Cost = \frac{P_{H2}}{\eta_{H2} . Q_{lhv}} + s . P_{bat} . penalty \tag{20}$$

The constraints are mentioned in Equations (2)–(6).

To prevent nitrogen power from being too small, especially when *SOC* is low, we added a dynamic lower bound:

$$P_{H_2 - min} = \text{min_}ratio * P_{demand} \tag{21}$$

where *min_ratio* is determined as follows:

$$\begin{aligned} &if\ SOC \leq 30\%,\ \text{min_ratio} = 0.7 \\ &if\ SOC \leq 50\%,\ \text{min_ratio} = 0.4 \\ &if\ SOC > 50\%,\ \text{min_ratio} = 0.1 \end{aligned}$$

This ensures that even with high solar power or high SOC, nitrogen contributes at least 10% of P_{demand}. Furthermore, at low *SOC* (e.g., 30%), nitrogen contributes up to 70%.

To add the influence of solar energy (*PV*), we implemented a 1D Lookup in Table 3:

Table 3. PV-based scaling factors applied to hydrogen power in the ECMS framework.

PV (kW)	Multiplier (on P_{H_2})
0.0	1.0 (full H_2 use)
0.4	0.95
0.7	0.85
1.0	0.7 (reduce H_2 use)

Then,

$$P_{H_2-final} = P_{H_2} \cdot PV\ factor \quad (22)$$

The optimization loop in the code tests a range of possible values for P_{H_2}, choosing the one with the minimum cost.

The system's behavior is summarized as shown in Table 4:

Table 4. Summary of ECMS power-sharing behavior under different SOC and PV conditions.

Conditions	Behavior
Low SOC (e.g., 30%)	Hydrogen dominates the power supply
High SOC (e.g., 80%)	Battery shares more load
Low PV (e.g., <400 W)	More hydrogen used
High PV (e.g., 1 kW)	Reduced hydrogen consumption

According to the constraints and cost function of the *EMS* of this study, the flowchart of *ECMS* is given in Figure 9.

As shown in Section 6.2, the *ECMS* maximized fuel economy by saving 10 L of hydrogen compared to the *PID* controller under sunny conditions. Conversely, the ANN provided the most stable operation, maintaining a final *SOC* above 80% with a standard deviation of only 1.2% in fluctuations.

4.5. Artificial Neural Network (ANN)

The network is trained using datasets covering different operating conditions. Table 5 summarizes the data intervals used for training the ANN, including ranges for *SOC*, PV power, and power demand generating the reference fuel cell power (*PFC*). The network is trained using datasets covering different operating conditions. The ANN strategy employs a multilayer perceptron architecture trained on simulation-generated datasets covering 45 distinct scenarios. This offline training method ensures that the controller can map real-time inputs (*SOC*, *PV* power, and P_{demand}) to optimal power-splitting commands with minimal online computational overhead.

Table 5. Preparing measurements for use as neural network inputs [66].

Measured Size	Range of Variation	Numbering Intervals for Specifying Neural Network Inputs
Battery *SOC*	$SOC \leq 33\%$	1
	$33\% < SOC \leq 66\%$	2
	$SOC > 66\%$	3
PV power	$PV \leq 33\%$	1
	$33\% < PV \leq 66\%$	2
	$PV > 66\%$	3

Table 5. *Cont.*

Measured Size	Range of Variation	Numbering Intervals for Specifying Neural Network Inputs
Power demand	Power demand = 20 (Very Small)	1
	Power demand = 40 (Small)	2
	Power demand = 60 (Medium)	3
	Power demand = 80 (Large)	4
	Power demand = 100 (Very Large)	5

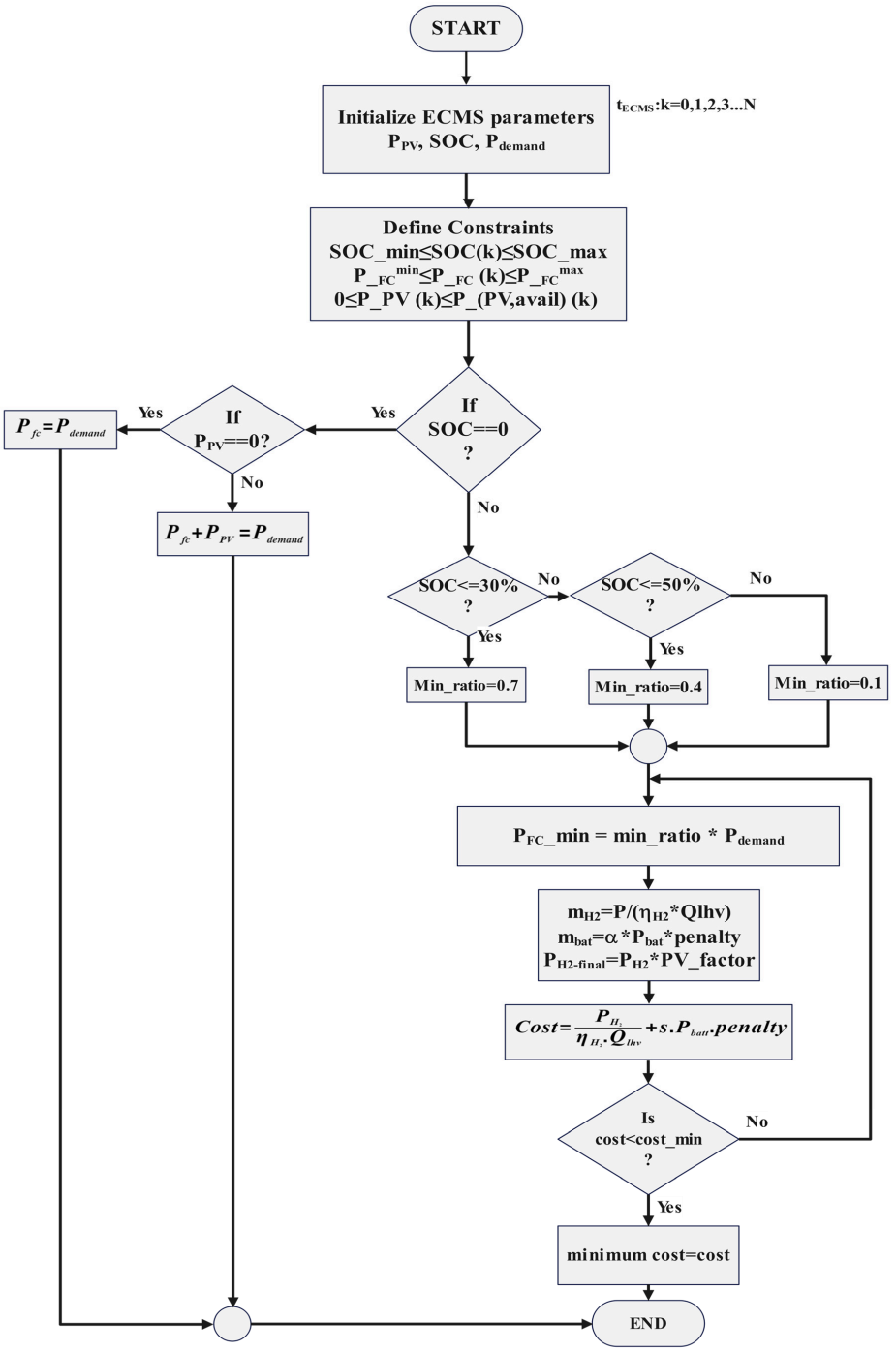


Figure 9. Flowchart of the Equivalent Consumption Minimization Strategy (*ECMS*) for real-time energy management.

Table 5 summarizes the data intervals used for training the ANN, including ranges for *SOC*, *PV* power, and power demand.

To satisfy the request for "specific parameter settings" for the ANN, we included the data classification used for the training input layers:

Battery *SOC* Intervals: ≤33% (Level 1), 33–66% (Level 2), >66% (Level 3).

PV Power Intervals: ≤33% (Level 1), 33–66% (Level 2), >66% (Level 3).

Power Demand (kW): Very Small (20), Small (40), Medium (60), Large (80), Very Large (100).

Figure 10 shows the architecture of the ANN, depicting the input, hidden, and output layers. Figure 11 presents the training data set used for the ANN, highlighting the distribution of input variables. Figure 12 illustrates the performance of the ANN controller in tracking reference fuel cell power.

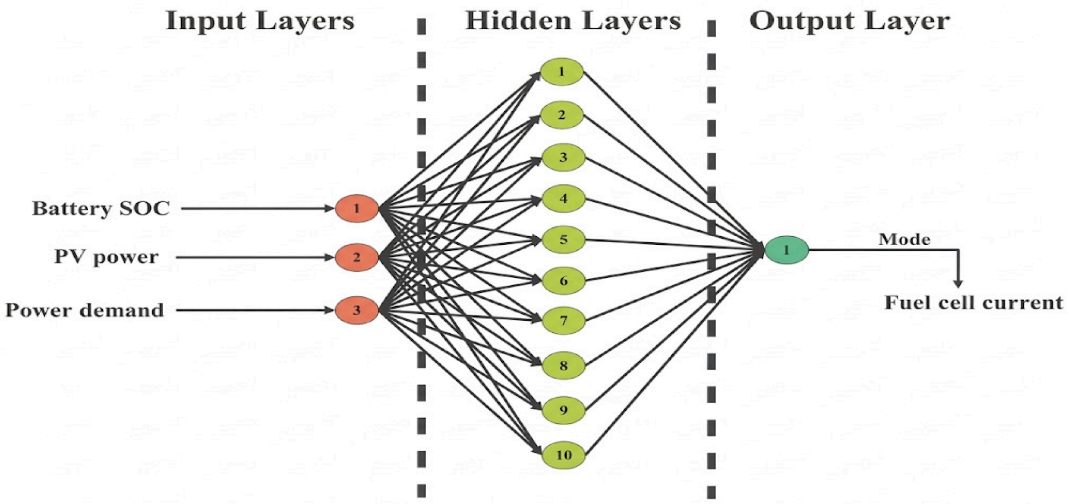


Figure 10. Neural network model architecture for power management.

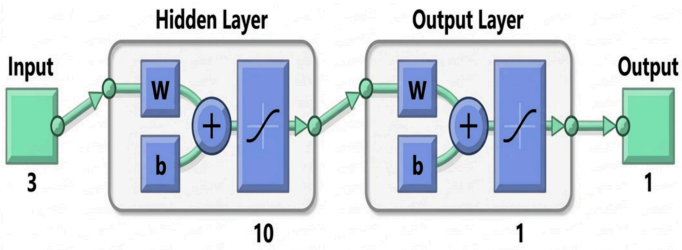


Figure 11. Neural network architecture for power management was implemented in MATLAB Simulink.

Table A1 summarizes the training data for the neural network-based learning method for the *EMS* of a *HEV* to be implemented in MATLAB/Simulink (R2018a).

4.6. Comparative Theoretical Expectations

Table 6 provides a comparative overview of the implemented Energy Management Strategies (*PID*, *FLC*, *ECMS*, *ANN*), highlighting their core principles, advantages, limitations, and key references. The table shows that the *PID* controller is fast and straightforward to tune but suffers from poor adaptability and high hydrogen consumption. The Fuzzy Logic Controller (*FLC*) offers robustness under uncertainty and balanced *SOC* but requires tuning and depends on a rule base. *ECMS* achieves the best fuel economy but may reduce *SOC* below safe thresholds. The Artificial Neural Network (ANN) provides stable *SOC* and adaptive control but requires a dataset and has a higher computational cost.

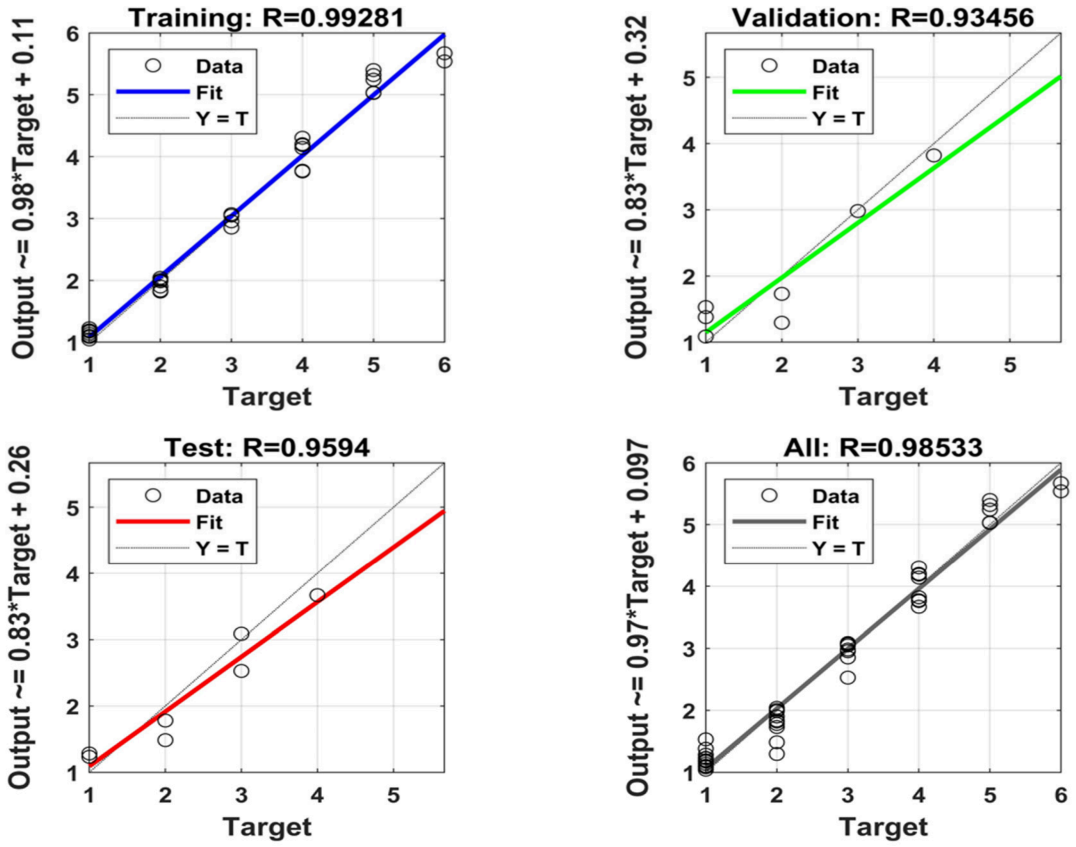


Figure 12. The target-driven training process.

Table 6. Comparative features of implemented Energy Management Strategies.

Strategy	Core Principle	Advantages	Limitations	Key References
PID	Feedback-based error correction	Simple, fast, easy to tune	Poor adaptability; high H_2 consumption	[77–81]
FLC	Rule-based linguistic decision	Robust under uncertainty; balanced SOC	Requires tuning; rule-based dependent	[16,82–89]
ECMS	Real-time fuel-equivalent minimization	Best fuel economy	Can reduce SOC below 50%	[26,90–93]
ANN	Data-driven predictive split	Stable SOC > 80%; adaptive	Needs dataset; computational cost	[36,94–96]

5. Simulation Scenarios and Test Conditions

5.1. Driving Cycle

The performance of the *PV–FC–HEV* was evaluated under the WLTP Class 1 driving cycle, which represents an 8.1 km mixed-speed profile. Figure 13 illustrates the WLTP Class 1 driving cycle, showing the vehicle speed and power demand profile used in the simulation.

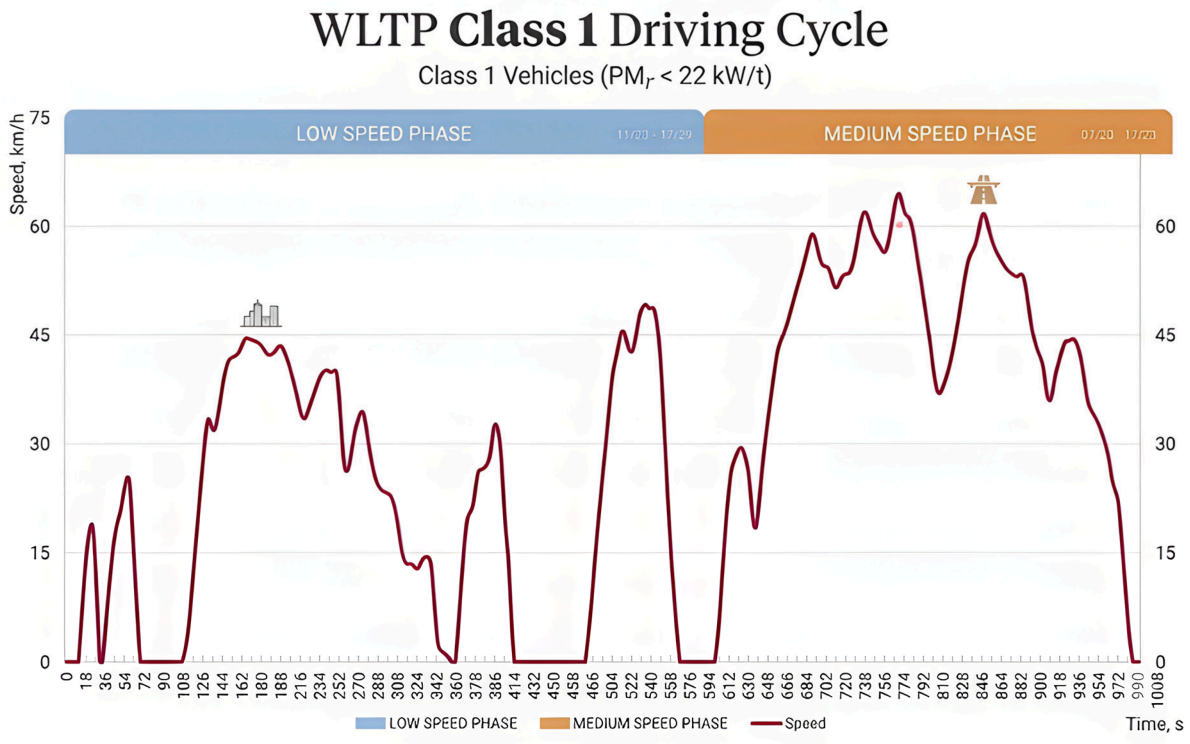


Figure 13. WLTP Class 1 driving cycle adopted for the *PV*–*FC*–Battery HEV simulations [97].

5.2. Irradiance-Based EMS Scenarios

Three main irradiance-based scenarios are considered for evaluating the EMS strategies:

- Sunny (1000 W/m^2, *SOC*_init = 80%): High *PV* contribution, initial *SOC* = 80%.
- Cloudy (400 W/m^2, *SOC*_init = 30%): Moderate *PV* input, initial *SOC* = 30%.
- Night (0 W/m^2, *SOC*_init = 50%): No *PV* input, initial *SOC* = 50%.

While 1000 W/m^2 represents Standard Test Conditions (*STC*), the level of 400 W/m^2 was specifically selected to simulate average cloudy conditions common in urban driving environments, rather than standard NOCT (800 W/m^2), to test the EMS's robustness under significantly reduced PV support and stressed battery conditions (initial *SOC* = 30%); Table 7 shows the description of these scenarios.

Table 7. Irradiance-based simulation scenarios used for EMS evaluation.

Scenario	Irradiance Level	Initial SOC	Description
Sunny	1000 W/m^2	80%	High solar input with strong *PV* contribution and high initial battery charge.
Cloudy	400 W/m^2	30%	Moderate irradiance with reduced *PV* support and stressed battery condition.
Night	0 W/m^2	50%	No solar irradiance: traction demand is supplied by the fuel cell and battery only.

6. Results and Comparative Analysis

This section summarizes and compares the main quantitative results for the four *EMS* strategies (*PID*, *FLC*, *ECMS*, *ANN*) applied to the *PV–FC–*Battery *HEV* under the considered irradiance and driving scenarios.

6.1. Comparative Results with Different Scenarios and Control Systems

6.1.1. Scenario 1 (Sunny: 1000 W/m^2)

In this scenario, the solar radiance is maintained at 1000 W/m^2. The PV array contributes to charging the battery, and the initial battery *SOC* reaches 80% when starting.

As shown in Figure 14A, the data indicates that the *PID* method leads to the highest hydrogen consumption, followed by Fuzzy Logic Control (*FLC*), then ANN control. The lowest consumption is observed with *ECMS*, with a noticeable difference of approximately 10 L between *PID* and *ECMS.* The difference in hydrogen usage is partly converted into electrical energy stored in the battery, which explains the relatively higher *SOC* levels in vehicles using *PID* and *FLC* strategies, as shown in Figure 14B. Although the ANN method maintained the highest *SOC* throughout most of the tests, it was not the most efficient in reducing fuel consumption. This highlights that the efficiency of energy conversion and distribution between the source and the battery varies with the chosen strategy, affecting overall performance and economic viability.

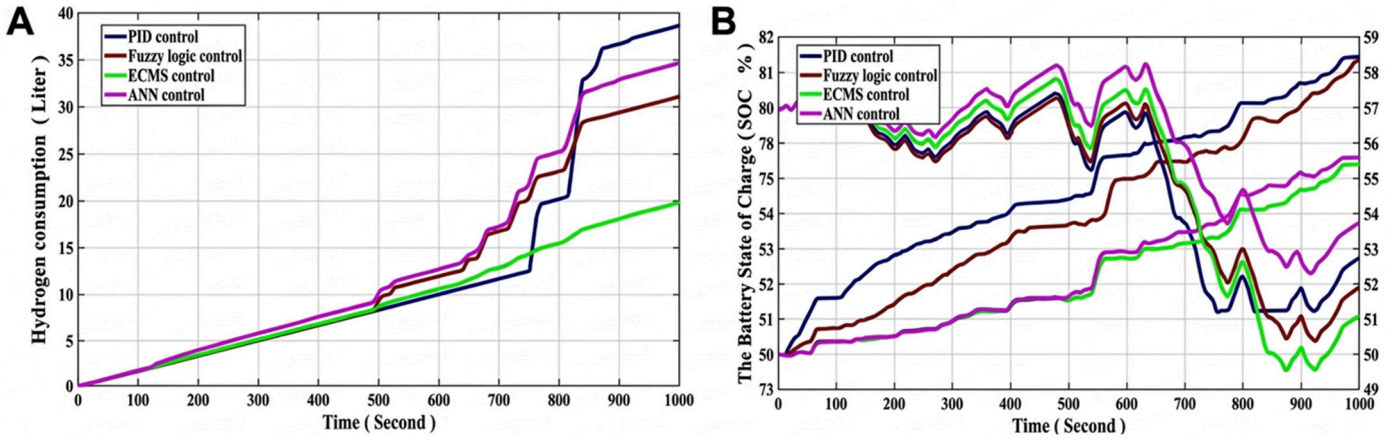


Figure 14. Comparison among *EMS* strategies in scenario 1: (**A**) hydrogen consumption (in liters), (**B**) battery *SOC* (%) [66].

6.1.2. Scenario 2 (Cloudy: 400 W/m^2)

This scenario is also a rainy condition where radiance is maintained at 400 W/m^2. *PV* power is insufficient in weak solar radiation, and the initial SOC of the battery is thirty percent.

As shown in Figure 15A, the *PID* strategy consumes the highest amount of hydrogen, followed by *FLC*, *ANN*, and finally *ECMS*, which remains the most efficient in terms of fuel usage. This increase in hydrogen consumption under low solar input reflects the need for an additional energy supply to support the battery charging process. In Figure 15B, the *SOC* increases steadily for all strategies, with *PID* achieving the highest *SOC* by the end of the cycle, followed by *FLC* and *ANN*, while *ECMS* lags. Although *ECMS* minimizes hydrogen consumption, it results in the lowest battery charge, highlighting the trade-off between fuel economy and energy availability. Overall, the selection of an energy management strategy under such weather conditions significantly influences both hydrogen usage and battery performance.

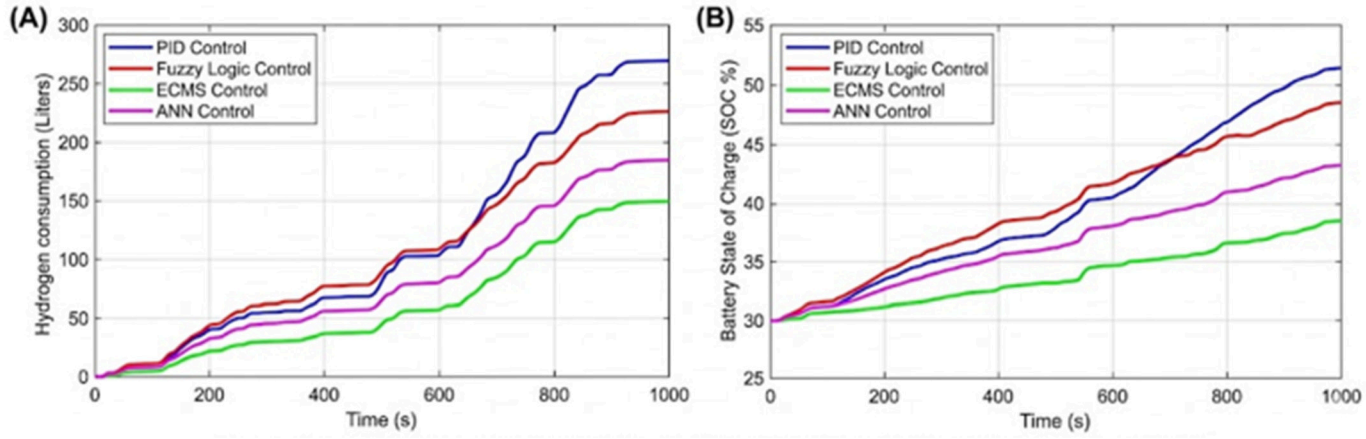


Figure 15. Comparison among *EMS* strategies in scenario 2: (**A**) hydrogen consumption (in liters), (**B**) battery *SOC* (%) [66].

6.1.3. Scenario 3 (Night/Dark: 00 W/m^2)

At nighttime, it is 0 W/m^2, which is the amount of sun radiation. Because the *PV* array is not functioning in this scenario, the only components that can provide power to the vehicle are the FC and the battery, and the initial *SOC* of the battery is fifty percent.

As shown in Figure 16A, the *PID* control strategy results in the highest hydrogen consumption, followed by *FLC*, *ECMS*, and *ANN* in descending order. This trend indicates that PID prioritizes maintaining power availability at the expense of increased hydrogen use, whereas ANN and *ECMS* strategies show better fuel economy. In Figure 16B, the *SOC* increases for all strategies, with *PID* maintaining the highest *SOC* throughout, followed by *FLC*. *ANN* shows the slowest *SOC* improvement, despite lower fuel use. These results highlight a trade-off between energy availability (*SOC* gain) and fuel efficiency across different EMS strategies in the absence of solar input. Choosing the optimal strategy thus depends on the desired balance between conserving hydrogen and ensuring sufficient battery performance.

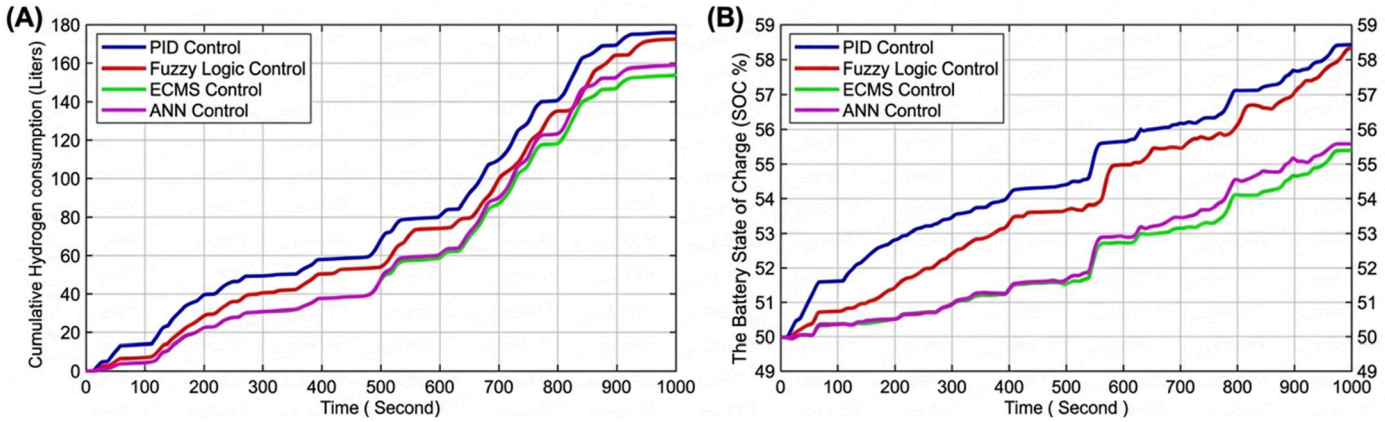


Figure 16. Comparison among *EMS* strategies in scenario 3: (**A**) hydrogen consumption (in liters), (**B**) battery *SOC* (%) [66].

Across all three conditions, the *PID* strategy consistently shows the highest hydrogen consumption but achieves the highest battery *SOC*. *FLC* and *ANN* strike a moderate balance between fuel economy and battery performance. *ECMS* stands out as the most fuel-efficient strategy but offers lower *SOC* gains. In sunny weather, solar input supports all strategies, but in cloudy or nighttime conditions, fuel efficiency becomes critical. *PID* prioritizes

energy availability, while others aim to optimize consumption. Overall, *ECMS* and *ANN* are better suited for long-term efficiency, especially under limited solar input.

6.2. Hydrogen Consumption Under Different EMS

Table 8 reports the hydrogen consumption and final battery *SOC* for *PID*, *FLC*, *ECMS*, and *ANN* under Sunny, Cloudy, and Night WLTP Class 1 conditions. Under Sunny operation, ECMS achieves the lowest hydrogen usage, whereas ANN maintains the highest final *SOC*, indicating a more conservative utilization of the battery. In the Cloudy case, ECMS still provides the best fuel-economy performance, while ANN preserves a relatively high SOC and thus a balanced trade-off between hydrogen saving and battery SOC swing amplitude. At night, when *PV* power is unavailable, all strategies rely mainly on the fuel cell, and the differences in hydrogen consumption become smaller, although PID remains the most hydrogen-intensive and ANN retains a modest *SOC* advantage. The proposed strategy was validated via Controller Hardware-in-the-Loop (CHiL) testing to ensure real-time execution stability.

Table 8. Comparative performance of four EMS control strategies under different scenarios.

Condition	Strategy	Hydrogen Consumption (L)	Final SOC (%)	Key Observation
Sunny (1000 W/m^2)	PID	42	82	Fast response: highest H_2 use
Sunny (1000 W/m^2)	FLC	36	80	Balanced operation
Sunny (1000 W/m^2)	ECMS	32	55	Best fuel saving (↓10 L vs. PID), SOC drop
Sunny (1000 W/m^2)	ANN	34	>80	Optimal trade-off
Cloudy (400 W/m^2)	PID	47	78	Over-compensation by FC
Cloudy (400 W/m^2)	FLC	43	75	Stable control
Cloudy (400 W/m^2)	ECMS	39	68	Efficient; deeper SOC loss
Cloudy (400 W/m^2)	ANN	41	79	Adaptive to low irradiance
Night (0 W/m^2)	PID	50	70	High H_2 consumption
Night (0 W/m^2)	FLC	47	68	Moderate efficiency
Night (0 W/m^2)	ECMS	44	65	Reduced H_2; lower SOC
Night (0 W/m^2)	ANN	45	73	Smooth transitions; balanced use

6.3. Power Distribution Analysis

Figure 17 presents consolidated power-flow and *SOC* profiles of the *PV–FC–*Battery *HEV* under Sunny, Cloudy, and Night conditions along the WLTP Class 1 cycle. Under high irradiance, *PV* power together with the battery supplies a substantial portion of the traction demand, allowing the fuel cell to operate at relatively low power and thus reducing hydrogen consumption. When irradiance decreases in the Cloudy case, the fuel cell contribution increases, and the EMS intermittently recharges the battery, leading to a gradual SOC rise. At night, *PV* generation is zero, so the fuel cell becomes the primary source, and the battery mainly buffers transient load peaks and absorbs regenerative braking; *ECMS* uses the battery more aggressively, ANN distributes power more evenly between fuel cell and battery, and *PID/FLC* occupy an intermediate position in terms of fuel-cell loading and battery support.

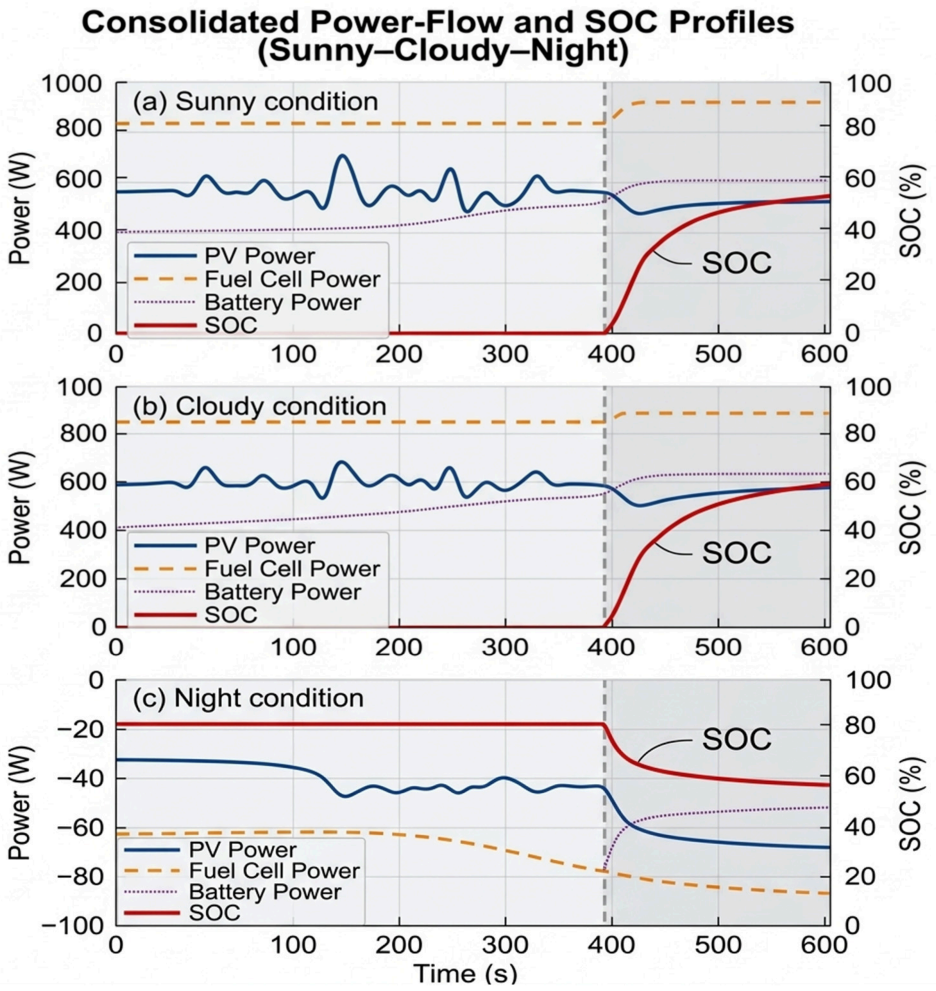


Figure 17. Consolidated power-flow and battery *SOC* profiles of the *PV–FC*–Battery HEV under Sunny, Cloudy, and Night irradiance conditions.

7. Conclusions

This study presented a comprehensive and comparative evaluation of four intelligent Energy Management Strategies (*EMS*)—*PID*, *FLC*, *ECMS*, and ANN—applied to a Photovoltaic–Fuel Cell–Battery hybrid electric vehicle (PV–FC–HEV).

A detailed MATLAB/Simulink model integrating dynamic vehicle, electrical, and control subsystems was developed to assess hydrogen consumption, battery state of charge (*SOC*), and power distribution under realistic driving and irradiance conditions.

Key findings can be summarized as follows: ECMS achieved the lowest hydrogen consumption, reducing fuel usage by up to 10 L under high solar irradiance (1000 W/m^2), confirming its superior efficiency in the hydrogen economy. ANN offers superior adaptability and improved *SOC* regulation, demonstrating a more conservative battery utilization profile compared to optimization-based strategies. These findings will further enhance adaptability and reduce hydrogen waste; future modeling of degradation dynamics is required to quantify impacts on service life. *FLC* demonstrated robust and smooth transitions under fluctuating irradiance, outperforming conventional *PID* control in both efficiency and adaptability. *PID* control, while simple and fast, recorded the highest hydrogen use and limited performance under dynamic loads, proving less suitable for renewable-integrated hybrid systems.

The comparative analysis reveals that *ECMS* is ideal for applications prioritizing fuel conservation, while ANN offers superior adaptability and improved SOC regulation, making it preferable for next-generation smart and sustainable *HEV* designs.

Future research will focus on hardware-in-the-loop (HIL) implementation to validate simulation outcomes under experimental conditions. Future work can also explore a vehicle-to-station collaborative energy management framework, linking vehicle control strategies with charging station scheduling to achieve network-level optimization of transportation energy of fuel-cell and battery systems in hybrid electric vehicles. Future work can also explore a vehicle-to-station collaborative energy management framework, linking vehicle control strategies with charging station scheduling to achieve network-level optimization of transportation energy.

Author Contributions: M.A.A.: Conceptualization, project administration, and primary supervision. R.A.S. and M.H.A.: Writing—original draft preparation, literature review, and data curation. M.M.: Theoretical framework development and validation of control strategies. S.A.: Software simulation and technical support. S.A.F. and H.Y.H.: Result verification, formal analysis, and writing—review and editing. All authors have read and agreed to the published version of the manuscript.

Funding: This research received no external funding.

Institutional Review Board Statement: Not applicable.

Informed Consent Statement: Not applicable.

Data Availability Statement: The datasets used during the current study are available from the corresponding author on reasonable request.

Acknowledgments: The Researchers would like to thank the Deanship of Graduate Studies and Scientific Research at Qassim University for financial support (QU-APC-2026).

Conflicts of Interest: The authors declare no conflicts of interest. The funders had no role in the design of the study; in the collection, analyses, or interpretation of data; in the writing of the manuscript; or in the decision to publish the results.

Appendix A

Table A1. Training table for ANN control strategy.

Operating Conditions	Inputs			Output	Operating Conditions	Inputs			Output
	Battery SOC	PV Power	Power Demand	Fuel Cell Current		Battery SOC	PV Power	Power Demand	Fuel Cell Current
S1	1	1	20	2	S24	3	1	60	2
S2	1	2	20	2	S25	3	2	60	1
S3	2	1	20	1	S26	2	3	60	2
S4	2	2	20	1	S27	3	3	60	1
S5	1	3	20	2	S28	1	1	80	5
S6	3	1	20	1	S29	1	2	80	5
S7	3	2	20	1	S30	2	1	80	4
S8	2	3	20	1	S31	2	2	80	4
S9	3	3	20	1	S32	1	3	80	4
S10	1	1	40	4	S33	3	1	80	2
S11	1	2	40	3	S34	3	2	80	2
S12	2	1	40	2	S35	2	3	80	3
S13	2	2	40	2	S36	3	3	80	1
S14	1	3	40	3	S37	1	1	100	6
S15	3	1	40	1	S38	1	2	100	6
S16	3	2	40	1	S39	2	1	100	5
S17	2	3	40	1	S40	2	2	100	4
S18	3	3	40	1	S41	1	3	100	5

Table A1. *Cont.*

Operating Conditions	Inputs			Output	Operating Conditions	Inputs			Output
	Battery SOC	PV Power	Power Demand	Fuel Cell Current		Battery SOC	PV Power	Power Demand	Fuel Cell Current
S19	1	1	60	5	S42	3	1	100	3
S20	1	2	60	4	S43	3	2	100	3
S21	2	1	60	3	S44	2	3	100	4
S22	2	2	60	3	S45	3	3	100	2
S23	1	3	60	4					

References

1. Jannesar Niri, A.; Poelzer, G.A.; Zhang, S.E.; Rosenkranz, J.; Pettersson, M.; Ghorbani, Y. Sustainability Challenges throughout the Electric Vehicle Battery Value Chain. *Renew. Sustain. Energy Rev.* **2024**, *191*, 114176. [CrossRef]
2. Ramachandaramurthy, V.K.; Ajmal, A.M.; Kasinathan, P.; Tan, K.M.; Yong, J.Y.; Vinoth, R. Social Acceptance and Preference of EV Users—A Review. *IEEE Access* **2023**, *11*, 11956–11972. [CrossRef]
3. Zhang, F.; Wang, L.; Coskun, S.; Pang, H.; Cui, Y.; Xi, J. Energy Management Strategies for Hybrid Electric Vehicles: Review, Classification, Comparison, and Outlook. *Energies* **2020**, *13*, 3352. [CrossRef]
4. Chandra Tella, V.; Alzayed, M.; Chaoui, H. A Comprehensive Review of Energy Management Strategies in Hybrid Electric Vehicles: Comparative Analysis and Challenges. *IEEE Access* **2024**, *12*, 181858–181878. [CrossRef]
5. Lü, X.; Qu, Y.; Wang, Y.; Qin, C.; Liu, G. A Comprehensive Review on Hybrid Power System for PEMFC-HEV: Issues and Strategies. *Energy Convers. Manag.* **2018**, *171*, 1273–1291. [CrossRef]
6. Podder, A.K.; Chakraborty, O.; Islam, S.; Manoj Kumar, N.; Alhelou, H.H. Control Strategies of Different Hybrid Energy Storage Systems for Electric Vehicles Applications. *IEEE Access* **2021**, *9*, 51865–51895. [CrossRef]
7. Ogulcan Parlak, B.; Ayhan Yavasoglu, H. Assessment of Vehicle-Integrated Photovoltaics: A Financial and Environmental Perspective. *Sustain. Energy Technol. Assess.* **2024**, *72*, 104042. [CrossRef]
8. Ray, S.; Kasturi, K.; Nayak, M.R. Multi-Objective Electric Vehicle Charge Scheduling for Photovoltaic and Battery Energy Storage Based Electric Vehicle Charging Stations in Distribution Network. *Green Energy Intell. Transp.* **2025**, *4*, 100296. [CrossRef]
9. Feng, G.; Feng, Z.; Sun, P.; Guo, L.; Chen, Z. A Overview of Energy Management Strategies for Hybrid Power Systems. *Energies* **2025**, *18*, 4769. [CrossRef]
10. Moulik, B.; Söffker, D. Optimal Rule-Based Power Management for Online, Real-Time Applications in HEVs with Multiple Sources and Objectives: A Review. *Energies* **2015**, *8*, 9049–9063. [CrossRef]
11. Cao, Y.; Yao, M.; Sun, X. An Overview of Modelling and Energy Management Strategies for Hybrid Electric Vehicles. *Appl. Sci.* **2023**, *13*, 5947. [CrossRef]
12. Wang, Y.; Tan, H.; Wu, Y.; Peng, J. Hybrid Electric Vehicle Energy Management With Computer Vision and Deep Reinforcement Learning. *IEEE Trans. Ind. Inf.* **2021**, *17*, 3857–3868. [CrossRef]
13. Ehsani, M.; Gao, Y.; Gay, S.E.; Emadi, A. *Modern Electric, Hybrid Electric, and Fuel Cell Vehicles: Fundamentals, Theory, and Design*; CRC Press: Boca Raton, FL, USA, 2004; ISBN 978-0-429-12819-6.
14. Fares, D.; Chedid, R.; Karaki, S.; Jabr, R.; Panik, F.; Gabele, H.; Huang, Y. Optimal Power Allocation for a FCHV Based on Linear Programming and PID Controller. *Int. J. Hydrogen Energy* **2014**, *39*, 21724–21738. [CrossRef]
15. Zhang, F.; Hu, X.; Langari, R.; Cao, D. Energy Management Strategies of Connected HEVs and PHEVs: Recent Progress and Outlook. *Prog. Energy Combust. Sci.* **2019**, *73*, 235–256. [CrossRef]
16. Maghfiroh, H.; Wahyunggoro, O.; Cahyadi, A.I. Energy Management in Hybrid Electric and Hybrid Energy Storage System Vehicles: A Fuzzy Logic Controller Review. *IEEE Access* **2024**, *12*, 56097–56109. [CrossRef]
17. Deng, L.; Radzi, M.A.M.; Shafie, S.; Hassan, M.K. Optimizing Energy Management in Fuel Cell Hybrid Electric Vehicles Using Fuzzy Logic Control with State Machine Approach: Enhancing SOC Stability and Fuel Economy. *J. Eng. Res.* **2025**, *13*, 3429–3440. [CrossRef]
18. Tao, C.W.; Taur, J.-S. Flexible Complexity Reduced PID-like Fuzzy Controllers. *IEEE Trans. Syst. Man Cybern. B* **2000**, *30*, 510–516. [CrossRef]
19. Gao, D.; Jin, Z.; Lu, Q. Energy Management Strategy Based on Fuzzy Logic for a Fuel Cell Hybrid Bus. *J. Power Sources* **2008**, *185*, 311–317. [CrossRef]
20. Bai, M.; Yang, W.; Zhang, R.; Kosuda, M.; Korba, P.; Hovanec, M. Fuzzy-Based Optimal Energy Management Strategy of Series Hybrid-Electric Propulsion System for UAVs. *J. Energy Storage* **2023**, *68*, 107712. [CrossRef]
21. Lee, H.-D.; Koo, L.-S.; Sul, S.-K.; Kim, J.-S. Torque Control Strategy for a Parallel-Hybrid Vehicle Using Fuzzy Logic. *IEEE Ind. Appl. Mag.* **2000**, *6*, 33–38. [CrossRef]

22. Brahma, A.; Glenn, B.; Guezennec, Y.; Miller, T.; Rizzoni, G.; Washington, G. Modeling, Performance Analysis and Control Design of a Hybrid Sport-Utility Vehicle. In *Proceedings of 1999 IEEE International Conference on Control Applications (Cat. No.99CH36328)*; IEEE: Kohala Coast, HI, USA, 1999; Volume 1, pp. 448–453.
23. Baumann, B.M.; Washington, G.; Glenn, B.C.; Rizzoni, G. Mechatronic Design and Control of Hybrid Electric Vehicles. *IEEE/ASME Trans. Mechatron.* **2000**, *5*, 58–72. [CrossRef]
24. Paganelli, G.; Delprat, S.; Guerra, T.M.; Rimaux, J.; Santin, J.J. Equivalent Consumption Minimization Strategy for Parallel Hybrid Powertrains. In *Proceedings of the Vehicular Technology Conference. IEEE 55th Vehicular Technology Conference. VTC Spring 2002 (Cat. No.02CH37367)*; IEEE: Birmingham, AL, USA, 2002; Volume 4, pp. 2076–2081.
25. Zhou, B.; Burl, J.B.; Rezaei, A. Rezaei Equivalent Consumption Minimization Strategy with Consideration of Battery Aging for Parallel Hybrid Electric Vehicles. *IEEE Access* **2020**, *8*, 204770–204781. [CrossRef]
26. Chai, H.; Zhao, X.; Yu, Q.; Wang, S.; Han, Q.; Zheng, Z. Adaptive Equivalent Consumption Minimization Strategy Based on Road Grade Estimation for a Plug-in Hybrid Electric Truck. *J. Energy Storage* **2023**, *70*, 108035. [CrossRef]
27. Ni, D.; Yao, C.; Zheng, X.; Huang, Q.; Luo, D.; Sun, F. Equivalent Consumption Minimization Strategy of Hybrid Electric Vehicle Integrated with Driving Cycle Prediction Method. *Machines* **2023**, *11*, 576. [CrossRef]
28. Fang, Z.; Chen, Z.; Yu, Q.; Zhang, B.; Yang, R. Online Power Management Strategy for Plug-in Hybrid Electric Vehicles Based on Deep Reinforcement Learning and Driving Cycle Reconstruction. *Green Energy Intell. Transp.* **2022**, *1*, 100016. [CrossRef]
29. Udeogu, C.U.; Lim, W. Improved Deep Learning-Based Energy Management Strategy for Battery-Supercapacitor Hybrid Electric Vehicle With Adaptive Velocity Prediction. *IEEE Access* **2022**, *10*, 133789–133802. [CrossRef]
30. Zhu, Z.; Liu, Y.; Canova, M. Energy Management of Hybrid Electric Vehicles via Deep Q-Networks. In *Proceedings of the 2020 American Control Conference (ACC)*; IEEE: Denver, CO, USA, 2020; pp. 3077–3082.
31. Millo, F.; Rolando, L.; Tresca, L.; Pulvirenti, L. Development of a Neural Network-Based Energy Management System for a Plug-in Hybrid Electric Vehicle. *Transp. Eng.* **2023**, *11*, 100156. [CrossRef]
32. Afzal, S.; Ziapour, B.M.; Shokri, A.; Shakibi, H.; Sobhani, B. Building Energy Consumption Prediction Using Multilayer Perceptron Neural Network-Assisted Models; Comparison of Different Optimization Algorithms. *Energy* **2023**, *282*, 128446. [CrossRef]
33. Aksan, F.; Suresh, V.; Janik, P. PV Generation Prediction Using Multilayer Perceptron and Data Clustering for Energy Management Support. *Energies* **2025**, *18*, 1378. [CrossRef]
34. Xie, S.; Hu, X.; Qi, S.; Lang, K. An Artificial Neural Network-Enhanced Energy Management Strategy for Plug-in Hybrid Electric Vehicles. *Energy* **2018**, *163*, 837–848. [CrossRef]
35. Kalaivani, P.; Joice, C.S. Design and Modelling of a Neural Network-Based Energy Management System for Solar PV, Fuel Cell, Battery and Ultracapacitor-Based Hybrid Electric Vehicle. *Electr. Eng.* **2024**, *106*, 689–709. [CrossRef]
36. Huang, B.; Yu, W.; Ma, M.; Wei, X.; Wang, G. Artificial-Intelligence-Based Energy Management Strategies for Hybrid Electric Vehicles: A Comprehensive Review. *Energies* **2025**, *18*, 3600. [CrossRef]
37. Ezzat, M.F.; Dincer, I. Development, Analysis and Assessment of a Fuel Cell and Solar Photovoltaic System Powered Vehicle. *Energy Convers. Manag.* **2016**, *129*, 284–292. [CrossRef]
38. Kojima, T.; Ishizu, T.; Horiba, T.; Yoshikawa, M. Development of Lithium-Ion Battery for Fuel Cell Hybrid Electric Vehicle Application. *J. Power Sources* **2009**, *189*, 859–863. [CrossRef]
39. Cairns, E.J.; Albertus, P. Batteries for Electric and Hybrid-Electric Vehicles. *Annu. Rev. Chem. Biomol. Eng.* **2010**, *1*, 299–320. [CrossRef]
40. Zhang, Z.; Fan, Y.; Tian, J.; Kuang, H.; Li, M.; Pan, T.; Wang, Y.; Liu, X. Online Estimation of Model Parameters and State of Charge for Lithium-Ion Battery Using Multitimescale Recurrent Neural Networks. *IEEE Trans. Ind. Electron.* **2025**, *72*, 8119–8129. [CrossRef]
41. Mokrani, Z.; Rekioua, D.; Rekioua, T. Modeling, Control and Power Management of Hybrid Photovoltaic Fuel Cells with Battery Bank Supplying Electric Vehicle. *Int. J. Hydrogen Energy* **2014**, *39*, 15178–15187. [CrossRef]
42. Zhang, R.; Li, X.; Sun, C.; Yang, S.; Tian, Y.; Tian, J. State of Charge and Temperature Joint Estimation Based on Ultrasonic Reflection Waves for Lithium-Ion Battery Applications. *Batteries* **2023**, *9*, 335. [CrossRef]
43. Adebanjo, I.T.; Eko, J.; Agbeyegbe, A.G.; Yuk, S.F.; Cowart, S.V.; Nagelli, E.A.; Burpo, F.J.; Allen, J.L.; Tran, D.T.; Bhattarai, N.; et al. A Comprehensive Review of Lithium-Ion Battery Components Degradation and Operational Considerations: A Safety Perspective. *Energy Adv.* **2025**, *4*, 820–877. [CrossRef]
44. Guo, J.; Li, Y.; Pedersen, K.; Stroe, D.-I. Lithium-Ion Battery Operation, Degradation, and Aging Mechanism in Electric Vehicles: An Overview. *Energies* **2021**, *14*, 5220. [CrossRef]
45. Fanoro, M.; Božanić, M.; Sinha, S. A Review of the Impact of Battery Degradation on Energy Management Systems with a Special Emphasis on Electric Vehicles. *Energies* **2022**, *15*, 5889. [CrossRef]
46. Liu, Y.; Lai, X.; Zheng, Y.; Cheng, E.; Zhu, J.; Qian, L. Recent Advancements and Perspectives in Lithium-Ion Battery Aging: Mechanism, Characterization, and Prediction. *J. Energy Storage* **2025**, *122*, 116670. [CrossRef]

47. Han, X.; Lu, L.; Zheng, Y.; Feng, X.; Li, Z.; Li, J.; Ouyang, M. A Review on the Key Issues of the Lithium Ion Battery Degradation among the Whole Life Cycle. *eTransportation* **2019**, *1*, 100005. [CrossRef]
48. Collath, N.; Tepe, B.; Englberger, S.; Jossen, A.; Hesse, H. Aging Aware Operation of Lithium-Ion Battery Energy Storage Systems: A Review. *J. Energy Storage* **2022**, *55*, 105634. [CrossRef]
49. Vega–Garita, V.; Heydarzadeh, M.; Dadash, A.H.; Immonen, E. The Need for Aging-Aware Control Methods in Lithium-Ion Batteries: A Review. *J. Energy Storage* **2025**, *132*, 117653. [CrossRef]
50. Parthasarathy, C.; Laaksonen, H.; Redondo-Iglesias, E.; Pelissier, S. Aging Aware Adaptive Control of Li-Ion Battery Energy Storage System for Flexibility Services Provision. *J. Energy Storage* **2023**, *57*, 106268. [CrossRef]
51. Yi, F.; Lu, D.; Wang, X.; Pan, C.; Tao, Y.; Zhou, J.; Zhao, C. Energy Management Strategy for Hybrid Energy Storage Electric Vehicles Based on Pontryagin's Minimum Principle Considering Battery Degradation. *Sustainability* **2022**, *14*, 1214. [CrossRef]
52. Meng, X.; Mei, J.; Tang, X.; Jiang, J.; Sun, C.; Song, K. The Degradation Prediction of Proton Exchange Membrane Fuel Cell Performance Based on a Transformer Model. *Energies* **2024**, *17*, 3050. [CrossRef]
53. Tang, X.; Zhang, Y.; Xu, S. Temperature Sensitivity Characteristics of PEM Fuel Cell and Output Performance Improvement Based on Optimal Active Temperature Control. *Int. J. Heat Mass Transf.* **2023**, *206*, 123966. [CrossRef]
54. Kanani, H.; Shams, M.; Hasheminasab, M.; Bozorgnezhad, A. Model Development and Optimization of Operating Conditions to Maximize PEMFC Performance by Response Surface Methodology. *Energy Convers. Manag.* **2015**, *93*, 9–22. [CrossRef]
55. Mayur, M.; Gerard, M.; Schott, P.; Bessler, W.G. Lifetime Prediction of a Polymer Electrolyte Membrane Fuel Cell under Automotive Load Cycling Using a Physically-Based Catalyst Degradation Model. *Energies* **2018**, *11*, 2054. [CrossRef]
56. Xiao, L.; Bian, M.; Sun, Y.; Yuan, J.; Wen, X. Transport Properties Evaluation of Pore-Scale GDLs for PEMFC Using Orthogonal Design Method. *Appl. Energy* **2024**, *357*, 122445. [CrossRef]
57. Jia, C.; He, H.; Zhou, J.; Li, K.; Li, J.; Wei, Z. A Performance Degradation Prediction Model for PEMFC Based on Bi-Directional Long Short-Term Memory and Multi-Head Self-Attention Mechanism. *Int. J. Hydrogen Energy* **2024**, *60*, 133–146. [CrossRef]
58. Sulaiman, N.; Hannan, M.A.; Mohamed, A.; Ker, P.J.; Majlan, E.H.; Wan Daud, W.R. Optimization of Energy Management System for Fuel-Cell Hybrid Electric Vehicles: Issues and Recommendations. *Appl. Energy* **2018**, *228*, 2061–2079. [CrossRef]
59. Han, R.; He, H.; Wang, Y.; Wang, Y. Reinforcement Learning Based Energy Management Strategy for Fuel Cell Hybrid Electric Vehicles. *Chin. J. Mech. Eng.* **2025**, *38*, 66. [CrossRef]
60. Du, C.; Huang, S.; Jiang, Y.; Wu, D.; Li, Y. Optimization of Energy Management Strategy for Fuel Cell Hybrid Electric Vehicles Based on Dynamic Programming. *Energies* **2022**, *15*, 4325. [CrossRef]
61. Jui, J.J.; Ahmad, M.A.; Molla, M.M.I.; Rashid, M.I.M. Optimal Energy Management Strategies for Hybrid Electric Vehicles: A Recent Survey of Machine Learning Approaches. *J. Eng. Res.* **2024**, *12*, 454–467. [CrossRef]
62. Arsad, A.Z.; Zuhdi, A.W.M.; Azhar, A.D.; Chau, C.F.; Ghazali, A. Advancements in Maximum Power Point Tracking for Solar Charge Controllers. *Renew. Sustain. Energy Rev.* **2025**, *210*, 115208. [CrossRef]
63. Baba, A.O.; Liu, G.; Chen, X. Classification and Evaluation Review of Maximum Power Point Tracking Methods. *Sustain. Futures* **2020**, *2*, 100020. [CrossRef]
64. Abedin, T.; Pasupuleti, J.; Paw, J.K.S.; Tak, Y.C.; Mahmud, M.; Abdullah, M.P.; Nur-E-Alam, M. Proton Exchange Membrane Fuel Cells in Electric Vehicles: Innovations, Challenges, and Pathways to Sustainability. *J. Power Sources* **2025**, *640*, 236769. [CrossRef]
65. Mubin, A.N.A.; Bahrom, M.H.; Azri, M.; Ibrahim, Z.; Rahim, N.A.; Raihan, S.R.S. Analysis Performance of Proton Exchange Membrane Fuel Cell (PEMFC). *IOP Conf. Ser. Mater. Sci. Eng.* **2017**, *210*, 012052. [CrossRef]
66. Sayed, R.A.; Allam, S.; Iqbal, S.; Shafiullah, M.; Aurangzeb, M.; Youssef Hegazy, H.; Abdel Fattah, S. Optimal Design and Simulation of an Artificial Neural Network Control System to Optimize Energy Management in a Hybrid Electric Vehicle. *J. Electr. Syst.* **2025**, *21*, 208–235.
67. Azzouzi, M.; Popescu, D.; Bouchahdane, M. Modeling of Electrical Characteristics of Photovoltaic Cell Considering Single-Diode Model. *J. Clean Energy Technol.* **2016**, *4*, 414–420. [CrossRef]
68. Nouri, L.; Ihfa, F.Z.; Oubella, Y.A.; Sakhi, Z.; Bennai, M. Single-Diode Multi-Junction Solar Cell Models Five-Parameter Estimation Method. *Indian J. Phys.* **2024**, *98*, 629–637. [CrossRef]
69. Saldaña, G.; San Martín, J.I.; Zamora, I.; Asensio, F.J.; Oñederra, O. Analysis of the Current Electric Battery Models for Electric Vehicle Simulation. *Energies* **2019**, *12*, 2750. [CrossRef]
70. Ajao, Q.M.; Sadeeq, L.G.; Oludamilare, O.; Qasim, M. An Overview of Lithium-Ion Battery Dynamics for Autonomous Electric Vehicles: A MATLAB Simulation Model. *Open Access Libr. J.* **2023**, *10*, e10272. [CrossRef]
71. Tang, X.; Chen, J.; Qin, Y.; Liu, T.; Yang, K.; Khajepour, A.; Li, S. Reinforcement Learning-Based Energy Management for Hybrid Power Systems: State-of-the-Art Survey, Review, and Perspectives. *Chin. J. Mech. Eng.* **2024**, *37*, 43. [CrossRef]
72. Beni Hamed, S.; Ben Hamed, M. Modeling and Simulation of a Proton Exchange Membrane Fuel Cell Stacks in MATLAB/SIMULINK Under Conditions Variations. In *Proceedings of the 2nd International Conference on Green Energy Conversion System*; Mellit, A., Sbita, L., Kemih, K., Ghanes, M., Eds.; Springer Nature: Singapore, 2024; pp. 255–266.

73. Mlazi, N.J.; Mayengo, M.; Lyakurwa, G.; Kichonge, B. Mathematical Modeling and Extraction of Parameters of Solar Photovoltaic Module Based on Modified Newton–Raphson Method. *Results Phys.* **2024**, *57*, 107364. [CrossRef]
74. Fan, C.; Liu, K.; Ren, Y.; Peng, Q. Characterization and Identification towards Dynamic-Based Electrical Modeling of Lithium-Ion Batteries. *J. Energy Chem.* **2024**, *92*, 738–758. [CrossRef]
75. Yu, H.; Chen, Y.-H.; Sun, L.; Zhou, Y.; Wang, Z.-R. Design and Experimental Validation of Permanent Magnet Motor for Propeller Aerodynamic Noise Test. *IEEE Access* **2023**, *11*, 125396–125410. [CrossRef]
76. Hwang, J.J.; Wang, D.Y.; Shih, N.C. Development of a Lightweight Fuel Cell Vehicle. *J. Power Sources* **2005**, *141*, 108–115. [CrossRef]
77. Borase, R.P.; Maghade, D.K.; Sondkar, S.Y.; Pawar, S.N. A Review of PID Control, Tuning Methods and Applications. *Int. J. Dynam. Control* **2021**, *9*, 818–827. [CrossRef]
78. Yu, S.; Li, X. Proportional–Integral–Derivative Controller Performance Assessment and Retuning Based on General Process Response Data. *ACS Omega* **2021**, *6*, 10207–10223. [CrossRef]
79. Dormido, S. Advanced PID Control. *IEEE Control Syst. Mag.* **2006**, *26*, 98–101. [CrossRef]
80. Samosir, A.S.; Sutikno, T.; Mardiyah, L. Simple Formula for Designing the PID Controller of a DC-DC Buck Converter. *Int. J. Power Electron. Drive Syst.* **2023**, *14*, 327. [CrossRef]
81. Sanchis, R.; Romero, J.A.; Balaguer, P. A Simple Procedure to Design PID Controllers in the Frequency Domain. In Proceedings of the 2009 35th Annual Conference of IEEE Industrial Electronics, Porto, Portugal, 3 November 2009; pp. 1420–1425.
82. Roumila, Z.; Rekioua, D.; Rekioua, T. Energy Management Based Fuzzy Logic Controller of Hybrid System Wind/Photovoltaic/Diesel with Storage Battery. *Int. J. Hydrogen Energy* **2017**, *42*, 19525–19535. [CrossRef]
83. Guler, N.; Ismail, Z.M.; Hazem, Z.B.; Naik, N. Adaptive Fuzzy Logic Controller-Based Intelligent Energy Management System Scheme for Hybrid Electric Vehicles. *IEEE Access* **2024**, *12*, 173441–173454. [CrossRef]
84. Li, Q.; Chen, W.; Li, Y.; Liu, S.; Huang, J. Energy Management Strategy for Fuel Cell/Battery/Ultracapacitor Hybrid Vehicle Based on Fuzzy Logic. *Int. J. Electr. Power Energy Syst.* **2012**, *43*, 514–525. [CrossRef]
85. Karuppa Samy, A.; Jeyadevi, S. Fuzzy Logic Based Battery Power Management for PV and Wind Hybrid Power System. *Asian J. Sci. Appl. Technol.* **2014**, *3*, 21–27. [CrossRef]
86. Seng, U.K.; Malik, H.; García Márquez, F.P.; Alotaibi, M.A.; Afthanorhan, A. Fuzzy Logic-Based Intelligent Energy Management Framework for Hybrid PV-Wind-Battery System: A Case Study of Commercial Building in Malaysia. *J. Energy Storage* **2024**, *102*, 114109. [CrossRef]
87. Doskéocil, R. Fuzzy Logic: An Instrument for the Evaluation of Project Status. *Rev. Métodos Cuantitativos Econ. Empresa* **2015**, *19*, 5–23.
88. Guler, N.; Hazem, Z.B.; Gunes, A. Optimizing Solar PV Systems Using Fuzzy Logic for Climate-Resilient Healthcare Infrastructure in Kyrgyzstan. *Green Technol. Sustain.* **2025**, *3*, 100190. [CrossRef]
89. Ferreira, A.A.; Pomilio, J.A.; Spiazzi, G.; de Araujo Silva, L. Energy Management Fuzzy Logic Supervisory for Electric Vehicle Power Supplies System. *IEEE Trans. Power Electron.* **2008**, *23*, 107–115. [CrossRef]
90. Ghadbane, H.E.; Mohamed, A.F. Optimizing Fuel Economy in Hybrid Electric Vehicles Using the Equivalent Consumption Minimization Strategy Based on the Arithmetic Optimization Algorithm. *Mathematics* **2025**, *13*, 1504. [CrossRef]
91. Zhang, Y.; Li, Q.; Wen, C.; Liu, M.; Yang, X.; Xu, H.; Li, J. Predictive Equivalent Consumption Minimization Strategy Based on Driving Pattern Personalized Reconstruction. *Appl. Energy* **2024**, *367*, 123424. [CrossRef]
92. García, P.; Torreglosa, J.P.; Fernández, L.M.; Jurado, F. Viability Study of a FC-Battery-SC Tramway Controlled by Equivalent Consumption Minimization Strategy. *Int. J. Hydrogen Energy* **2012**, *37*, 9368–9382. [CrossRef]
93. Motapon, S.N.; Dessaint, L.-A.; Al-Haddad, K. A Robust H_2-Consumption-Minimization-Based Energy Management Strategy for a Fuel Cell Hybrid Emergency Power System of More Electric Aircraft. *IEEE Trans. Ind. Electron.* **2014**, *61*, 6148–6156. [CrossRef]
94. Michailidis, P.; Michailidis, I.; Gkelios, S.; Kosmatopoulos, E. Artificial Neural Network Applications for Energy Management in Buildings: Current Trends and Future Directions. *Energies* **2024**, *17*, 570. [CrossRef]
95. Carranza-Abaid, A.; Jakobsen, J.P. Neural Network Programming: Integrating First Principles into Machine Learning Models. *Comput. Chem. Eng.* **2022**, *163*, 107858. [CrossRef]
96. Bourenane, H.; Berkani, A.; Negadi, K.; Marignetti, F.; Hebri, K. Artificial Neural Networks Based Power Management for a Battery/Supercapacitor and Integrated Photovoltaic Hybrid Storage System for Electric Vehicles. *J. Eur. Syst. Autom.* **2023**, *56*, 139–151. [CrossRef]
97. Lee, C.-M.; Lin, W.-S. Stochastic Self-Optimizing Power Management for Fuel Cell Hybrid Scooters of Different Sized Components. *Int. J. Hydrogen Energy* **2015**, *40*, 5197–5209. [CrossRef]

Disclaimer/Publisher's Note: The statements, opinions and data contained in all publications are solely those of the individual author(s) and contributor(s) and not of MDPI and/or the editor(s). MDPI and/or the editor(s) disclaim responsibility for any injury to people or property resulting from any ideas, methods, instructions or products referred to in the content.